ORNL/TM-2024/3659

SCALE Analyses of Scenarios in the Molten Salt Reactor Fuel Cycle

Donny Hartanto
Georgeta Radulescu
Friederike Bostelmann
William Wieselquist

Approved for public release.
Distribution is unlimited.

February 2025

OAK RIDGE National Laboratory

ORNL IS MANAGED BY UT-BATTELLE LLC FOR THE US DEPARTMENT OF ENERGY

ORNL/TM-2024/3659

Nuclear Energy and Fuel Cycle Division

SCALE ANALYSES OF SCENARIOS IN THE MOLTEN SALT REACTOR FUEL CYCLE

Donny Hartanto
Georgeta Radulescu
Friederike Bostelmann
William Wieselquist

February 5, 2025

Prepared by
OAK RIDGE NATIONAL LABORATORY
Oak Ridge, TN 37831
managed by
UT-BATTELLE LLC
for the
US DEPARTMENT OF ENERGY
under contract DE-AC05-00OR22725

CONTENTS

LIST OF FIGURES

LIST OF TABLES

LIST OF ABBREVIATIONS

AC	actinide
ALI	annual limit on intake
DAC	derived air concentration
EFPY	effective full-power year
FP	fission product
HALEU	high-assay low-enriched uranium
LT	light element
LWR	light-water reactor
MSBR	molten salt breeder reactor
MSR	molten salt reactor
MSRE	Molten Salt Reactor Experiment
MTIHM	metric ton initial heavy metal
non-LWR	non-light-water reactor
NRC	Nuclear Regulatory Commission
OGS	off-gas system
ORNL	Oak Ridge National Laboratory
PWR	pressurized water reactor
SNL	Sandia National Laboratories

ACKNOWLEDGMENTS

This work was supported by the US Nuclear Regulatory Commission, Office of Nuclear Regulatory Research, under Contract IAA 31310022S0011. The authors thank Steve Skutnik and Dane De Wet for the technical review of the report.

ABSTRACT

In support of the US Nuclear Regulatory Commission non-light-water reactor fuel cycle demonstration project, the capabilities of SCALE 6.3.1 for radionuclide characterization, criticality, and shielding were demonstrated through several scenarios in a molten salt reactor (MSR) nuclear fuel cycle. Three scenarios were selected for this study, with the molten salt breeder reactor (MSBR) serving as the reference design. The original thorium-based fuel salt used in MSBR was replaced with a ^{235}U-enriched fuel salt to better reflect anticipated future MSR concepts.

The first scenario focused on the fuel salt preparation stage. Criticality analyses, using SCALE/CSAS-Shift and SCALE/SAMPLER, examined potential critical configurations in the fresh fuel salt container based on variables such as ^{235}U enrichment, UF_4 molar fraction, temperature, and container geometry. The second scenario explored the release of fission products during reactor operation in which the tritium buildup in the primary fuel salt was quantified through depletion calculations using SCALE/TRITON with continuous fuel makeup and fractional fission product removal. This scenario also assessed radioactivity levels in the off-gas system (OGS), quantifying radiotoxic nuclides that could be released into the environment. SCALE/SAMPLER was employed to perform uncertainty quantification to identify key operating parameters influencing the buildup of radiotoxic nuclides in the OGS. Additionally, radiation dose rates were calculated using SCALE/MAVRIC to estimate the maximum exposure levels within the reactor cell complex during operation. The final scenario evaluated the decay heat and radioactivity of the primary fuel salt collected in the drain tank, as well as the radiation dose rate outside the building from the presence of the drain tank. Overall, the application of SCALE's various capabilities for radionuclide inventory generation, criticality analysis, and shielding in MSR fuel cycles was successfully demonstrated across these scenarios.

1. INTRODUCTION

In recent years, the advanced nuclear reactor technologies, particularly non-light-water reactors (non-LWRs), have gained significant attention because of their potential to improve safety, efficiency, and versatility. To support the licensing for these emerging technologies, the US Nuclear Regulatory Commission (NRC) has focused on assessing computational codes that are used to model accident progression, estimate source terms, and conduct consequence analysis to evaluate the safety and performance of non-LWRs in a wide range of operational and accident scenarios (US NRC 2020). A central aspect of these efforts has been the SCALE (Wieselquist and Lefebvre 2023) and MELCOR (Humphries et al. 2021) code systems. The SCALE code, developed by Oak Ridge National Laboratory (ORNL), is widely used for a variety of neutronics calculations, including for radionuclide characterization, reactor physics, criticality safety, and shielding analyses, alongside other applications. The MELCOR code, developed by Sandia National Laboratories (SNL), specializes in the detailed modeling of severe accident progression and source-term evaluation. Together, these codes provide a comprehensive framework for evaluating accident scenarios from the initial stages of progression to the release of radioactive materials. The integration of these codes to simulate relevant non-LWRs has been demonstrated for a variety of reactor designs, including heat pipe reactors (Walker et al. 2021; Wagner, Faucett, et al. 2022), high-temperature pebble-bed gas-cooled reactors (Wagner, Beeny, and Luxat 2022; Skutnik and Wieselquist 2021), fluoride-salt–cooled high-temperature reactors (Bostelmann et al. 2022; Wagner, Haskin, et al. 2022), molten-salt–fueled reactors (Lo et al. 2022; Wagner et al. 2023), and sodium-cooled fast reactors (Shaw et al. 2023; Wagner, Beeny, and Luxat 2023). As a result of these comprehensive evaluations, the best practices for using SCALE code to model the selected non-LWRs are detailed in Bostelmann et al. (2024).

Building on these initial efforts, the NRC continued with the next phase, aimed at demonstrating the capabilities of SCALE and MELCOR across all stages of the nuclear fuel cycle for non-LWRs (US NRC 2021). This task began with the development of representative nuclear fuel cycles for five distinct non-LWR designs, identifying potential hazards and accident scenarios at each stage (Bostelmann et al. 2023). Subsequently, specific accident scenarios were chosen to demonstrate the codes' capabilities, independent of the likelihood of occurrence. To date, two significant demonstrations have been documented: the first involving the nuclear fuel cycle of a high-temperature gas-cooled pebble-bed reactor (Elzohery et al. 2024), and the second focusing on the sodium-cooled fast reactor (Hartanto, Radulescu, et al. 2024). This report presents the third demonstration, centered on the nuclear fuel cycle of a molten salt reactor (MSR), using the molten salt breeder reactor (MSBR) (Robertson 1971) as a reference.

1.1 REFERENCE MOLTEN SALT REACTOR

The MSBR was selected as the reference design for this fuel cycle demonstration since it was intended for power generation, making it more representative of future commercial MSRs. Although the Molten Salt Reactor Experiment (MSRE) had previously been modeled using the SCALE code to demonstrate key features of the liquid-fueled MSR concept for source terms applications (Lo et al. 2022), its relatively small power of about 10 MWth is considered unrepresentative of future commercial MSRs. Additionally, the MSRE's fuel had a ^{235}U enrichment of 34.5 wt%, which is beyond the commonly considered maximum enrichment of 20 wt% for high-assay low-enriched uranium (HALEU) for currently pursued MSR concepts. In contrast, the MSBR was designed to operate at higher power of 2,250 MWth (1,000 MWe), making it a more representative and realistic model for accident progression studies. Furthermore, the MSBR benefits from a well-documented and detailed conceptual design (Robertson 1971), providing a solid reference for modeling.

The MSBR, developed in 1971 as part of the US Molten Salt Reactor Program, is a thermal-spectrum, liquid-fueled reactor that uses molten fluoride salts as both fuel and coolant. It was designed to operate at high temperatures with inherent safety features and to use the Th-^{233}U fuel cycle (Robertson 1971). The core configuration, as illustrated in Figure 1, is divided into two zones with distinct fuel-to-graphite volume ratios. Zone I, located in the inner core region where most of the fission occurs, has about 13% fuel salt-to-graphite moderator volume ratio. In this zone, four graphite control rods are positioned at the center of the core. When these rods are withdrawn, negative reactivity is introduced into the core because of the reduction in neutron moderation. Zone II, located in the outer core region, has a fuel-to-moderator volume ratio of ~37%, making it the primary breeding region. The fuel salt flows from the bottom to the top of the core, with inlet and outlet temperatures of 838.7 K and 977.6 K, respectively. The outer core region is also surrounded by a 30 in. graphite reflector. The reactor vessel is constructed from Hastelloy-N.

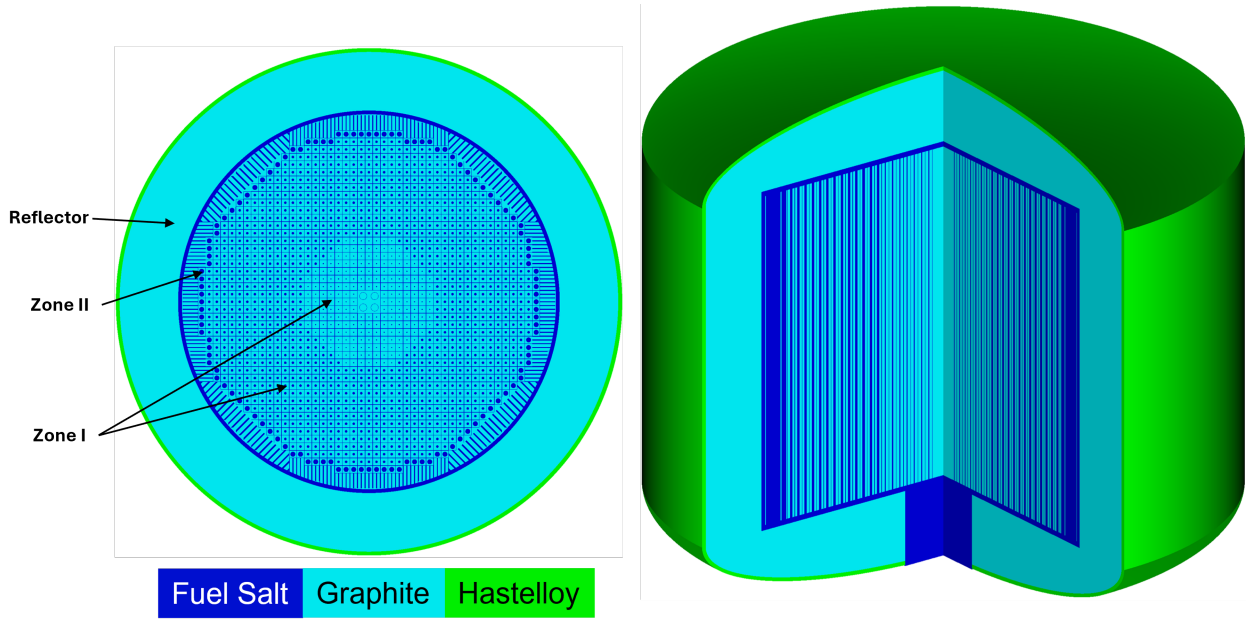

Figure 1. SCALE MSBR model.

To align with future MSR concepts for which license applications are expected in the near future, the original MSBR thorium-bearing fuel salt was replaced with a new composition based on ^{235}U-enriched fuel salt. Since most proposed graphite-moderated MSR designs use a mixture of UF_4 as fissile salt and FLiBe as the carrier salt, the first consideration was to use the MSRE fuel salt, ^{7}LiF-BeF_2-ZrF_4-UF_4 at 4.70-29.38-5.10-0.82 mol%. However, its low molar fraction of UF_4 resulted in a low initial heavy metal mass. Given that the thermal power of MSBR is ~225 times higher than that of the MSRE, using this composition would lead to an impractically high specific power. In this study, the composition ^{7}LiF-BeF_2-UF_4 at 60-30-10 mol% was proposed as the fuel salt, mixing only UF_4 and FLiBe. This composition was selected based on the FLiBe phase diagram using the data from the Molten Salt Thermal Properties Database (ORNL 2024), as depicted in Figure 2. This salt composition ensures a low melting point while maximizing uranium loading. Additionally, ^{7}Li was enriched to 99.995%, as found in common FLiBe specifications, to minimize tritium production and reduce the neutron absorption rate from ^{6}Li (Gehin and Powers 2016). Despite the change in the fuel salt composition, the core configuration and dimensions were retained from the initial design. The SCALE model for this demonstration was constructed by leveraging the model developed for a previous effort at ORNL (Davidson et al. 2021). Table 1 summarizes the main parameters of the reference MSR modeled used in this demonstration. The initial core requires ^{235}U enrichment of approximately 2.3 wt%,

providing an initial core excess reactivity of about 500 pcm. To sustain operation for 4 years, the enrichment of the makeup or feed fuel salt was set to 5.0 wt%, which is approximately double the initial salt enrichment.

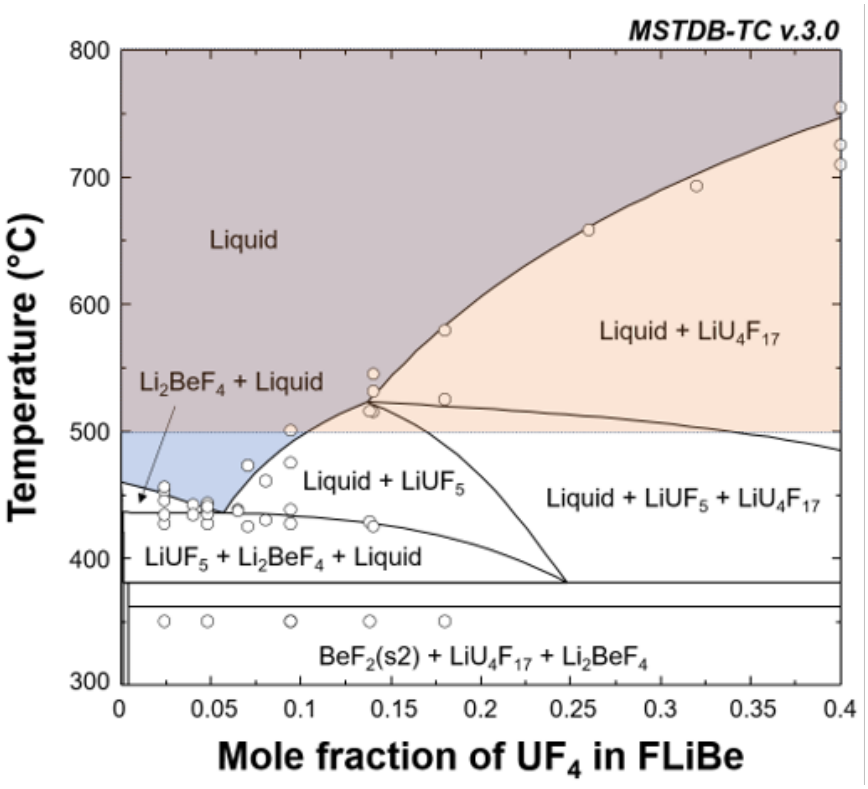

Figure 2. FLiBE phase diagram (Pinto 2024; ORNL 2024).

Table 1. Main design parameters of the reference MSR

Parameter	Value
Reactor power	2,250 MWth 1,000 MWe
Fuel composition	^{7}LiF-BeF_2-UF_4 60-30-10 mol%
^{235}U enrichment	2.3 wt% (fresh) 5.0 wt% (feed)
Fuel salt density	2.2488 g/cm^3
Total initial heavy metal	43.954 MT
Core lifetime	4 years

1.2 SELECTED ACCIDENT SCENARIOS

For this demonstration, three accident scenarios were selected from various stages of the MSR nuclear fuel cycle to be analyzed using the SCALE code that cover criticality, shielding, and decay heat (radionuclide inventory generation) analyses. The stages, corresponding accident scenarios, and the analyses are summarized as follows:

- **Fuel Salt Preparation Stage:** A criticality accident was assumed to occur because of insufficient mixing of fissile and carrier salts, resulting in batches with high concentrations of fissile material. Suitable fuel salt canisters were first identified, and criticality analyses were performed for different compositions, temperatures, and the identified canisters.
- **Reactor Operation Stage:** After four years of reactor operation, a release of fission products (FPs) was assumed. The amount of tritium produced during operation was quantified, along with its activity levels. FPs from the off-gas system (OGS) were also examined to assess the potential release of high-radiotoxicity nuclides and the impact of reactor operating parameters on their buildup. Radiation shielding calculations were conducted for the reactor cell complex, using the operating reactor as the radiation source. Depletion calculations were performed to determine the fuel inventory at the time of the accident.
- **Fuel Salt Drainage Stage:** This scenario considered a failure in the heat removal system of the drain tank after the core and the loop's entire fuel salt inventory was collected in the tank. Decay heat was evaluated, and shielding calculations were performed. The irradiated fuel inventory generated from the second scenario was used as the radiation source term for these analyses.

2. APPLIED SCALE SEQUENCES

The SCALE code is a comprehensive modeling and simulation suite for nuclear safety analysis and design (Wieselquist and Lefebvre 2023). The code includes verified and validated tools for criticality safety, reactor physics, radiation shielding, radioactive source characterization, and sensitivity and uncertainty analysis. The work described in this report was accomplished primarily using four sequences of SCALE.

- **CSAS:** The CSAS sequence is designed for criticality safety evaluations. It uses either the KENO or the Shift Monte Carlo code for neutron transport calculations. CSAS can evaluate the criticality of different configurations by calculating the effective multiplication factor k_{eff} under various conditions and configurations in systems such as fuel assemblies, reactor cores, or fuel storage configurations (Goluoglu et al. 2011).
- **TRITON:** TRITON is used for reactor physics and fuel depletion calculations to generate source term inventories. It couples neutron transport solvers using Monte Carlo methods, such as KENO or Shift, or solvers using deterministic methods, such as XSDRN or NEWT, with the ORIGEN depletion solver to model the evolution of isotopes during reactor operation. TRITON can simulate both 2D and 3D reactor configurations, making it suitable for analyzing fuel assemblies and entire reactor cores. It tracks the buildup of FPs, actinides, and other isotopes over time, providing detailed information on fuel behavior, radionuclide inventories, and decay heat (De Hart and Bowman 2011). A recently added feature of TRITON allows it to model a MSR by simulating the continuous feed of fresh fuel salt (e.g., to simulate refueling) and the removal of FPs (e.g., through the OGS) (Hartanto, Bostelmann, et al. 2024).
- **MAVRIC:** MAVRIC is used primarily for radiation shielding and dose analysis. It combines the Monaco or Shift Monte Carlo radiation transport code with an automated variance reduction method to improve the efficiency and accuracy of radiation transport simulations, especially in complex geometries (Peplow 2011). MAVRIC uses an importance map generated by the Denovo deterministic code to guide particle tracking in Monte Carlo simulations, significantly reducing computational time while maintaining precision (Evans et al. 2010). Radiation source terms determined using SCALE's depletion and decay modules can be accessed directly by MAVRIC, simplifying the input specifications.
- **SAMPLER:** SAMPLER is a powerful sequence used for uncertainty and sensitivity analysis. It introduces stochastic variations in nuclear data, system parameters, and modeling assumptions, enabling a comprehensive evaluation of uncertainties in results. SAMPLER integrates seamlessly with other SCALE sequences, such as TRITON and CSAS, to propagate uncertainties through reactor physics and criticality safety calculations. By sampling input parameters, including cross-section uncertainties, material compositions, and geometric perturbations, SAMPLER can quantify the impact of these uncertainties on key outputs such as k_{eff}, neutron flux distributions, isotope inventories, and decay heat.

All calculations documented in this report were performed using the continuous-energy Shift Monte Carlo code (Pandya et al. 2016) in combination with the ENDF/B-VII.1 nuclear data library (Chadwick et al. 2011).

3. SCENARIO 1: CRITICALITY EVENT DURING FUEL SALT PREPARATION

The preparation of enriched fresh fuel salt was modeled based on techniques used in the MSRE (Shaffer 1971). Because of the unavailability of recent data on fresh molten fuel salt preparation, the method employed in the MSRE was applied to the current scenario. In this process, batches of melted raw materials, specifically carrier salt FLiBe and fissile salt UF_4, were mixed in a treatment vessel and subsequently transferred to a storage vessel. The treatment consists of a Schelule 40 stainless steel pipe, the length and inner diameter of which are 36 in. and approximately 6 in., respectively, with an 1/8-in. thick inner liner of nickel. In contrast, the storage vessel consists of a Schedule 40 grade A nickel pipe, the length and inner diameter of which are 36 in. and approximately 4 in., respectively. Although both vessels had similar heights, the treatment vessel had a larger radius than the storage vessel. Additionally, the materials used for construction differed: the treatment vessel was constructed from stainless steel with a nickel liner, while the storage vessel was made entirely of nickel.

In this scenario, the criticality calculations were performed using SCALE/CSAS-Shift to identify the most unfavorable conditions for criticality. Model perturbations were explored using SCALE/SAMPLER for parameters that included the following:

- ^{235}U enrichment (nominal: 2.3 wt%)
- UF_4 molar fraction (nominal: 10 mol%)
- Temperature (nominal: room temperature, 300 K)
- Vessel radius (nominal: 8.41375 cm for the treatment vessel and 6.35 cm for the storage vessel (Shaffer 1971))

Simulations were conducted for both single-vessel configurations (using vacuum boundary conditions) and an infinite array of vessels (using reflective boundary conditions). In the latter case, the vessels were arranged in a tight hexagonal array configuration, with the vessels in contact (pitch-to-diameter ratio of 1.0). The SCALE models of the two vessels, along with their dimensions and the height of the fuel salt in each container, are shown in Figure 3.

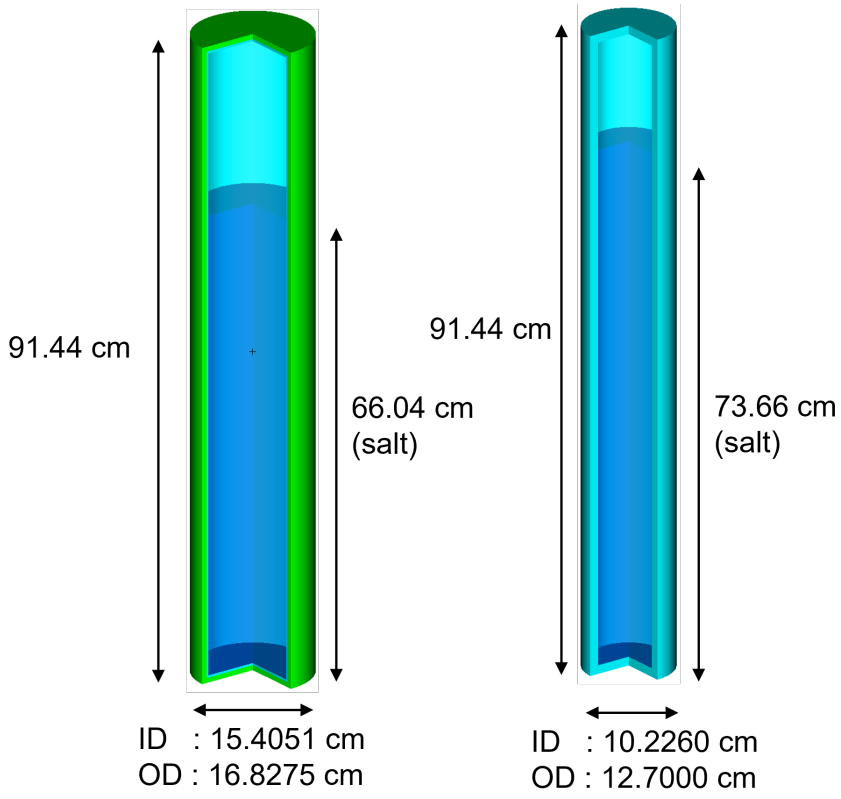

Figure 3. CSAS-Shift model for treatment (left) and storage (right) vessels.

3.1 CRITICALITY ANALYSIS

The first criticality analysis examined the impact of ^{235}U enrichment in UF_4 salt, as shown in Figure 4. The multiplication factor (k) was calculated for two configurations: (1) vessels containing pure UF_4 salt and (2) vessels containing a mixture of fuel salt and carrier salt, with UF_4 making up ~10 mol% of the mixture consistent with the fuel salt composition determined for this study (see Chapter 1). The results revealed that in an infinite array configuration the k for the treatment vessel containing pure UF_4 could approach or even exceed the critical safety limit of 0.95 when the enrichment surpassed 14 wt%. In contrast, the storage vessels, because of their smaller diameter, exhibited higher neutron leakage, causing them to reach the criticality safety threshold at a higher enrichment level of ~16 wt% for the infinite array configuration. To mitigate the risk of criticality in these scenarios, adopting a looser array configuration—with increased spacing between vessels—would reduce the k and enhance safety margins.

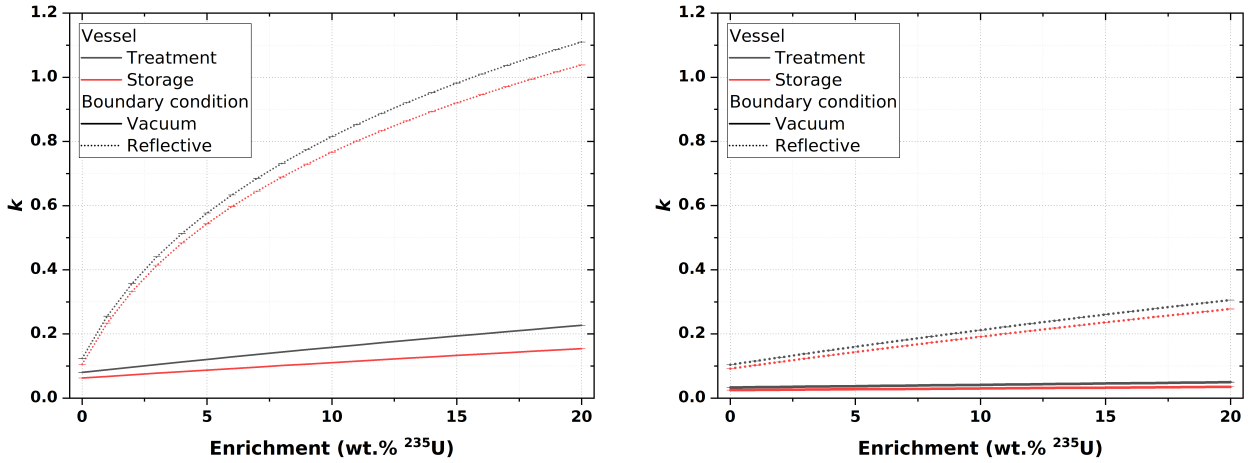

(a) UF_4 salt **(b) Mixture of FLiBe and UF_4 salt**

Figure 4. Multiplication factor of the vessels as a function of uranium enrichment.

The second perturbation focused on the effect of varying the molar fraction of UF_4 in both the treatment and storage vessels, with UF_4 fractions ranging up to 20 mol% and the ^{235}U enrichment set at a nominal value of 2.3 wt%. As shown in Figure 5, the trends in the multiplication factor for both types of vessels were very similar across all cases. Importantly, k remained consistently well below the critical safety limit of 0.95, regardless of the UF_4 molar fraction. This indicated that even with variations in the UF_4 molar fraction up to 20 mol%, the impact on criticality was minimal.

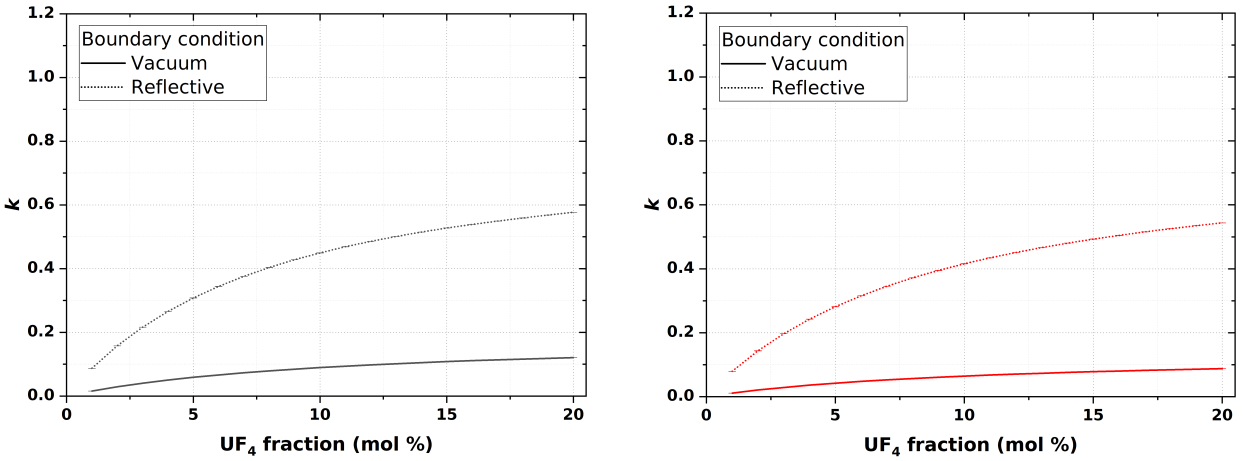

(a) Treatment vessel **(b) Storage vessel**

Figure 5. Multiplication factor of the vessels as a function of UF_4 molar fraction.

The third perturbation evaluated the effect of solution temperature on criticality for vessels containing both pure UF_4 salt and a mixture of fuel salt and carrier salt, each at a nominal ^{235}U enrichment of 2.3 wt%, with the results presented in Figure 6. As the solution temperature increased, the density of the solution, which was estimated based on additive molar volumes (Williams, Toth, and Clarno 2006), was updated accordingly to reflect the corresponding change in the physical properties. The results indicated a slight decrease in criticality as the temperature increased, with the k values for both vessel configurations consistently staying below the critical safety limit of 0.95. This slight reduction in criticality with increasing temperature can be attributed to the reduced density of the solution at higher temperatures. These results confirm that temperature variations within operational ranges have only a minor impact on criticality and do not significantly influence the overall safety of the system.

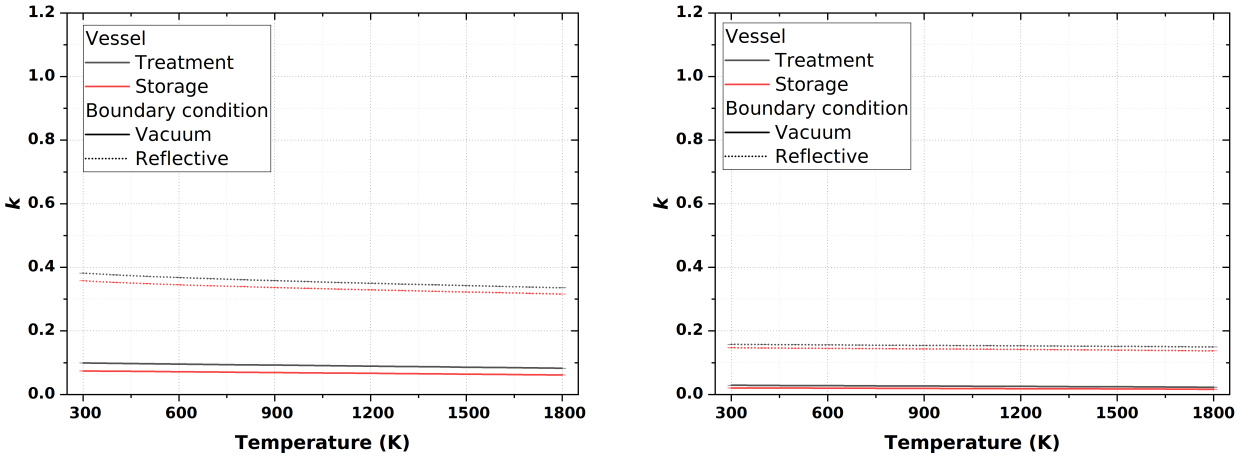

(a) UF_4 salt **(b) Mixture of FLiBe and UF_4 salt**

Figure 6. Multiplication factor of the vessels as a function of solution temperature.

The final perturbation examined the influence of vessel radius on criticality, with the results illustrated in Figure 7. In this case, the radii of both vessels containing UF_4 salt with an enrichment of 2.3 wt% were systematically increased. It was determined that this enrichment level was sufficient for achieving criticality

in the core simulations, as discussed in Section 4.1. However, across all cases, the k values remained below the critical safety limit of 0.95, demonstrating that even with an increase in vessel size, the system retained adequate safety margins. This indicates that the system is relatively insensitive to moderate changes in vessel dimensions for the current fresh fuel enrichment. The ability to adjust vessel dimensions within reasonable bounds without risking criticality provides flexibility in the operational scalability.

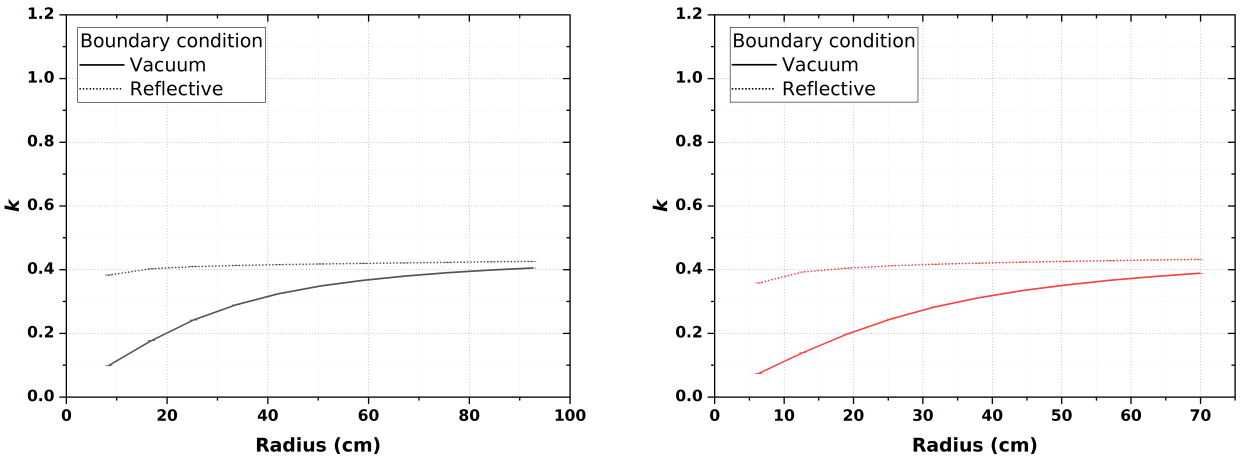

(a) Treatment vessel **(b) Storage vessel**

Figure 7. Multiplication factor of the vessels as a function of vessel radius.

Overall, the results from the criticality analyses demonstrated that the fresh fuel salt containers used in the MSRE exhibit excellent criticality safety margins under a range of perturbations, including variations in ^{235}U enrichment, UF_4 molar fraction, temperature, and vessel radius. It was observed that the criticality safety limit can be exceeded when the enrichment of the fuel salt surpasses 14 wt%, indicating the need for careful control in enrichment levels. Given that the initial enrichment of the fresh fuel composition for the reference core in this study is ~2.3 wt%, there is significant flexibility to adjust vessel dimensions within reasonable limits while maintaining criticality safety.

4. SCENARIO 2: RELEASE OF FISSION PRODUCTS DURING OPERATION

The release of FPs was modeled to occur after four years of continuous reactor operation in this scenario. Important FPs, as well as tritium, were assessed, with a focus on quantifying their production and activity level throughout the reactor's lifetime. The behavior of FPs within the OGS was also analyzed, specifically evaluating the release of highly radiotoxic nuclides and how reactor operating conditions influence their accumulation and potential activity. Additionally, radiation shielding evaluation was conducted within the reactor cell complex, treating the reactor itself as the primary radiation source. To accurately obtain the FPs at the point of the hypothetical release, depletion calculations were conducted first. This depleted inventory was then used as the radiation source for the subsequent shielding calculation.

4.1 DEPLETION CALCULATIONS

MSRs are designed for continuous operation, with fresh fuel salt continuously added to compensate for the depletion of fissile material through fission, as well as for the accumulation of neutron-absorbing fission and decay products. Consequently, the enrichment of the feed fuel salt is typically higher than that of the initial salt. Using more enriched fuel salt can reduce the total amount of added salt required. For example, in the MSRE, highly enriched uranium was introduced gradually by dissolving a eutectic mixture of ^{7}LiF-UF_4 from small capsules, which were mechanically lowered into the fuel pump (Robertson 1965).

In the reference MSR model of this study, the composition of the feed fuel salt remained the same as the initial salt, ^{7}LiF-BeF_2-UF_4 at 60-30-10 mol%, with the exception that the ^{235}U enrichment was increased to 5.0 wt%. This enrichment level was chosen to align with levels typically used in the current light-water reactors (LWRs). In SCALE/TRITON, the continuous addition of feed fuel salt in the depletion calculation can be specified in units of grams, kilograms, or moles per second. To determine the appropriate feed rate, a depletion calculation was performed for the target operation time of four effective full-power years (EFPYs), and the reduction in fissile nuclides was observed. The feed rate, in grams per second, was calculated by dividing the reduction of fissile nuclides by the total operating days. This calculated feed rate was then applied in a subsequent depletion calculation to confirm that the core's k_{eff} is approximately constant over time. Although SCALE/TRITON supports time-dependent feed rates, which can account for phenomena like xenon buildup after startup, this feature was not used in this study.

To maintain a constant volume of the fuel salt in the system (including the core and loop) during operation, a balance tank was modeled in the SCALE/TRITON simulation, as illustrated in Figure 8. This tank received excess fuel salt at the same rate that fresh fuel salt was introduced, ensuring the total system volume remained constant. This approach was necessary because SCALE/TRITON cannot currently consider changes in volume over time. Without such a balance tank, the addition of salt would lead to a nonphysical increase in fuel salt density. Modern MSR designs typically accommodate volume increase by using the extra space in the fuel loop, which is initially filled with inert gas, to avoid the need for salt removal during operation. The consideration of a fuel salt increase in the loop is a planned TRITON development effort.

In addition to modeling the fuel feed, the simulation in SCALE/TRITON also considered FP removal mechanisms such as removal of noble gases to the OGS and plating-out of the noble metals on structural materials. In the legacy MSBR technical report, the removal rates for noble gases and noble metals were $\sim 5.00 \times 10^{-2}$ 1/s (Robertson 1971). However, this study adopted a lower removal rate of 3.33×10^{-2} 1/s, following recent work from the SAMOSAFER Molten Fluoride Salt Reactor projects (Santora 2022). The removed noble gases included Xe and Kr, while the noble metals considered for plating out included Se, Nb, Mo, Tc, Ru, Rh, Pd, Ag, Sb, and Te. The implementation and pathways for fuel salt feeding and FP removal in the SCALE/TRITON are shown in Figure 8.

Note that redox potential control was not accounted for in this simulation. In actual MSR operation, the redox potential of the fuel salt is monitored continuously to prevent corrosion of structural materials. Corrosion mitigation is typically achieved by adding elements such as beryllium or uranium as buffer to the fuel salt, which helps maintain a stable redox environment and minimizes the corrosive effects on the reactor components. If information about required beryllium or uranium additions were available, it could be considered in the simulations using TRITON's feed capability.

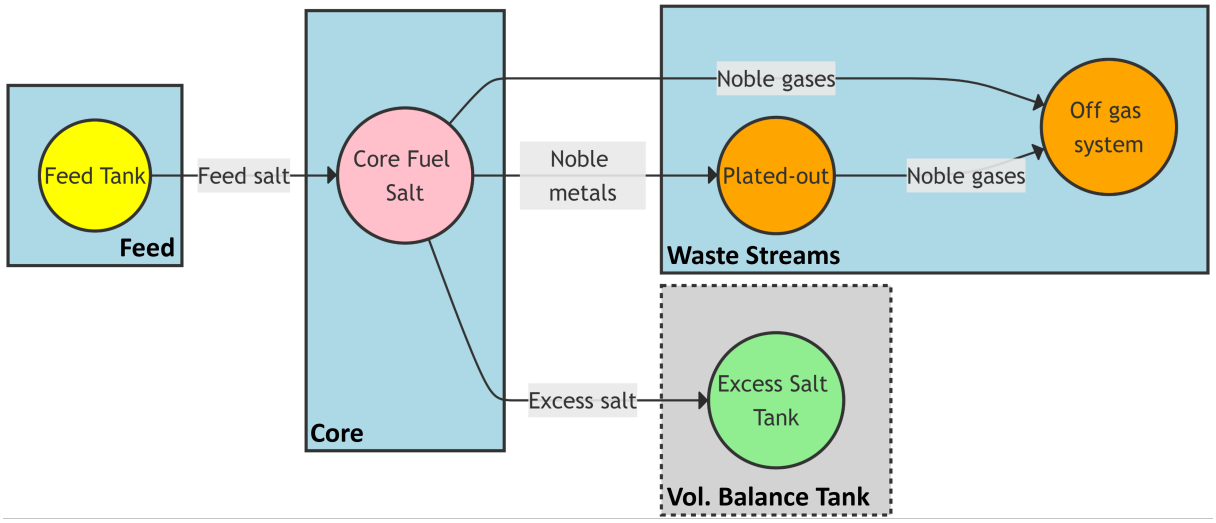

Figure 8. Fuel salt feed and FP removal paths implemented in SCALE/TRITON simulation.

Figure 9 shows the full-core neutron multiplication factor k_{eff} over time during a 4-EFPY cycle, with and without FP removal and/or refueling. Without refueling or FP removal, k_{eff} dropped significantly immediately after startup, primarily because of xenon buildup, a major neutron absorber. When FP removal, including xenon, was accounted for, the k_{eff} did not show the initial steep drop but instead decreased gradually over time. With constant refueling, k_{eff} remained approximately constant except for an initial bump caused by applying a constant feed rate, which temporarily introduced excess fissile material into the core. This effect dissipated after approximately half a year, as the FPs and transuranic actinides accumulated. Implementing a time-dependent or a batch-wise feed rate could prevent this behavior and maintain a constant k_{eff} throughout the operation.

After four EFPYs, a feed fuel salt volume (at 5 wt% ^{235}U enrichment) equal to ~3.5 times the total system's fuel salt volume was added to the core to remain critical. This large volume can be explained by the use of low enriched feed salt. Additionally, the use of a balance tank in the simulation, where excess fuel salt is stored, also contributed to this increased volume. In the SCALE/TRITON model, fuel addition and removal are applied to a single homogenized fuel mixture, meaning that any newly added fresh fuel is immediately mixed with the system's existing fuel salt. Since a small portion of the fuel was continuously removed to maintain a constant volume, some of the fresh fuel is also removed during this process. Using more highly enriched refueling salt would significantly reduce the total volume of feed fuel required. For instance, using a ^{235}U enrichment of 13.0~14.0 wt% enables the core remain critical over four EFPYs, while maintaining a refueling salt volume equal to the system's initial fuel salt volume, as illustrated in Figure 10.

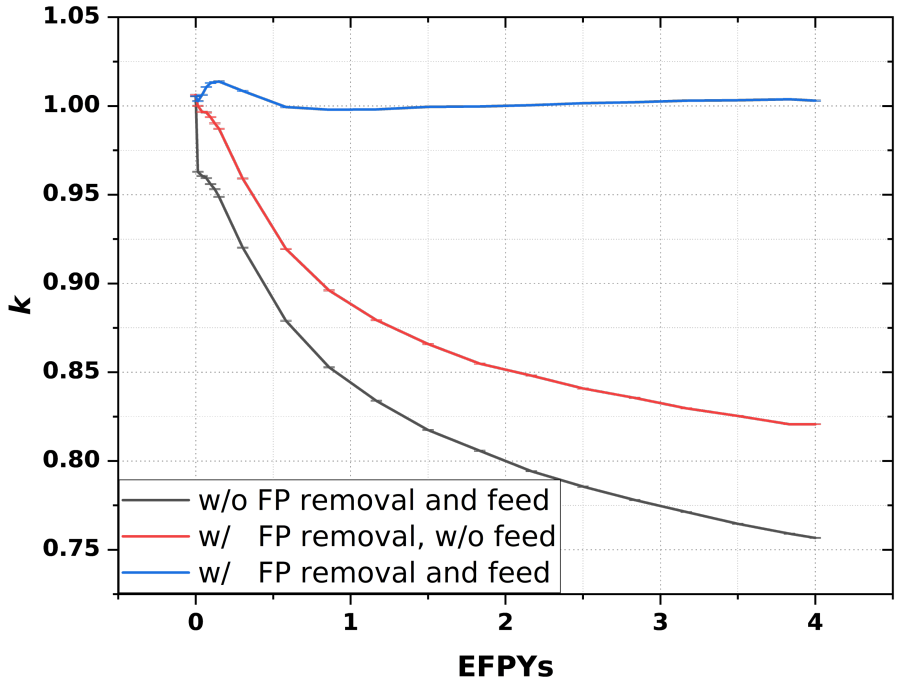

Figure 9. Evolution of k_{eff} with and without fission product removal and feed.

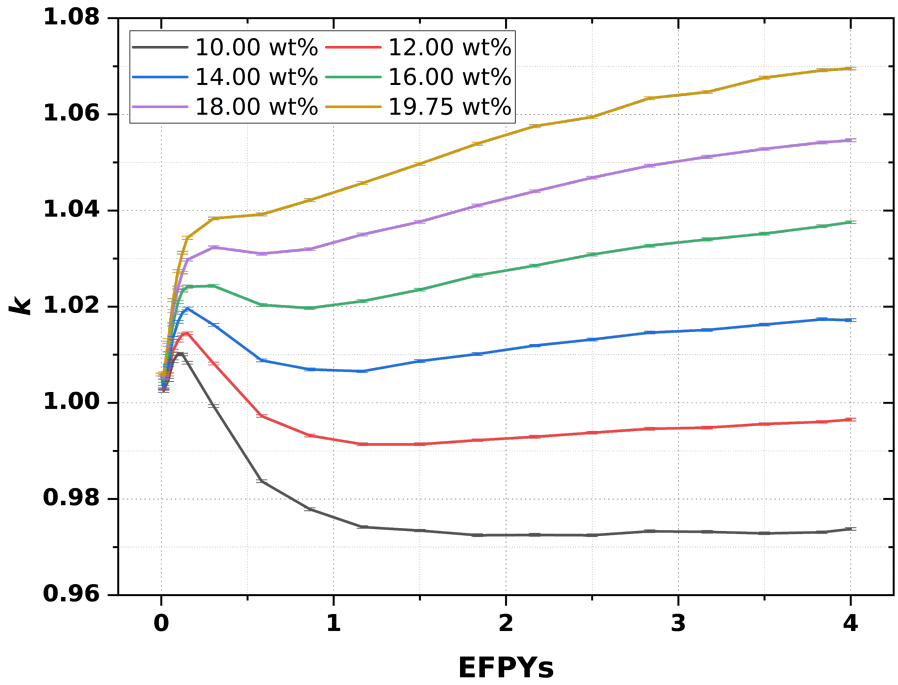

Figure 10. Evolution of k_{eff} for different feed enrichment, assuming the total feed volume over 4 years is equal to the initial fuel salt volume.

4.2 TRITIUM BUILDUP IN PRIMARY LOOP

Tritium (^{3}H) production is a notable concern in MSRs, particularly in those using FLiBe salt. Tritium is produced primarily through neutron capture reactions involving lithium, leading to substantial tritium accumulation over time (Dolan et al. 2021). The high operating temperatures in MSRs allow tritium to diffuse through reactor components, presenting a radiological hazard as it can permeate and escape from metallic structures. As a result, accurately assessing the potential amount of tritium that can be produced in an MSR is essential for the development and implementation of effective mitigation strategies. Techniques such as permeation barriers, helium sparging, or dedicated tritium capture systems can be used to minimize both operational and environmental risks associated with tritium release (Fuerst, Taylor, and Humrickhouse 2021; Gabraskas, Fei, and Jerden 2020).

In this study, the accumulation of tritium within the primary fuel salt after continuous reactor operation in the reference MSR model was estimated to be ~147 g of ^{3}H, as illustrated in Figure 11. This corresponds to a volumetric activity of ~38 Ci/L of fuel salt, as shown in Figure 12. The volumetric activity increase rate is approximately 8 Ci/L per year. Note that in this simulation, no tritium removal mechanism were incorporated, meaning all the tritium produced was assumed to remain within the system, except for losses due to radioactive decay. This assumption results in a more conservative estimation of tritium concentration compared to a reactor equipped with active tritium removal and control systems. The incorporation of such tritium removal mechanisms can be simulated in SCALE/TRITON, similar to the approach used for the removal of noble gases and noble metals.

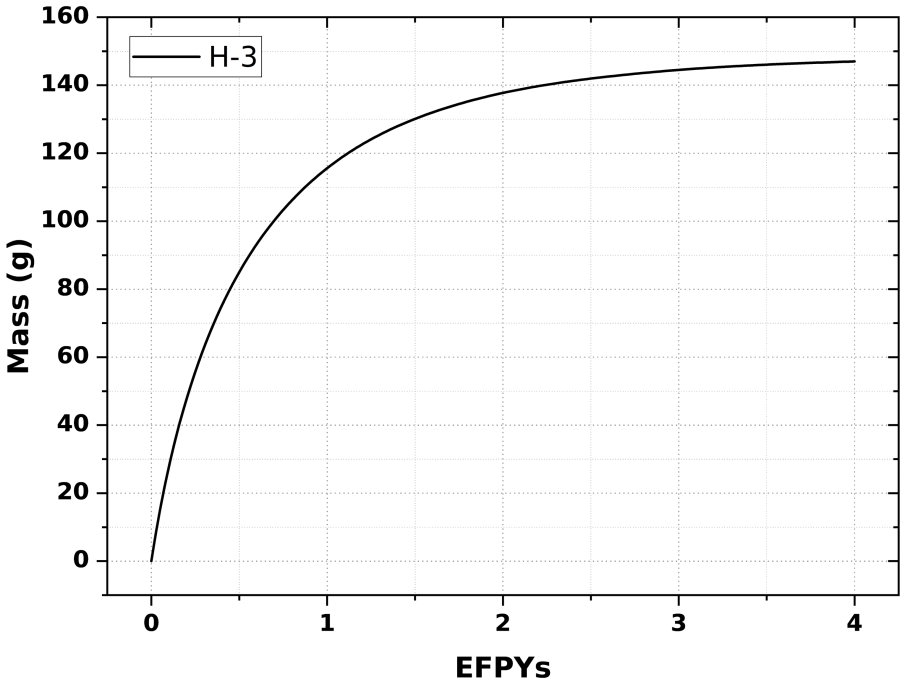

Figure 11. Buildup of tritium mass in primary loop.

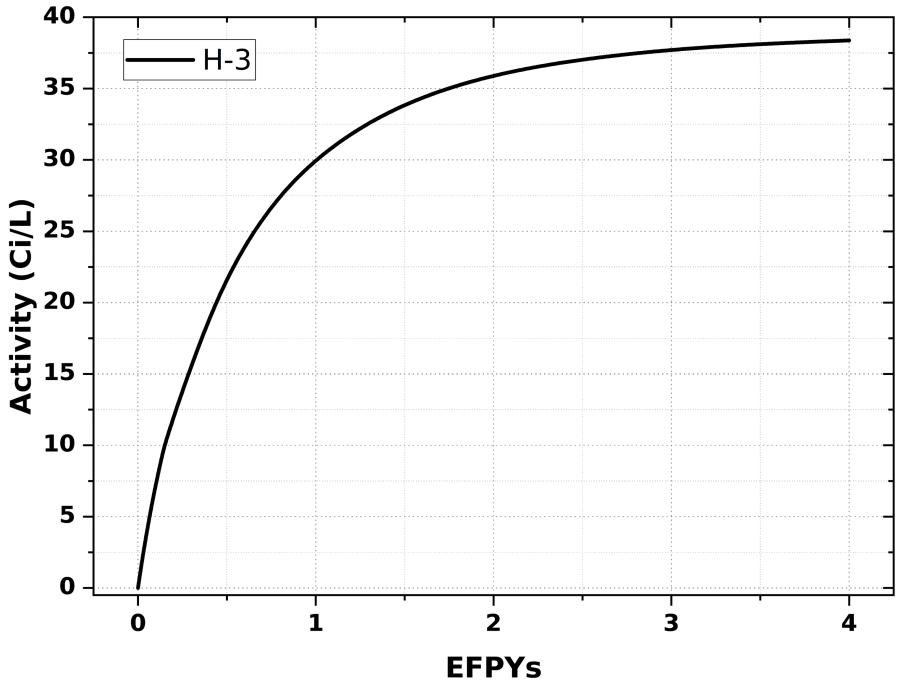

Figure 12. Buildup of tritium activity in primary loop.

4.3 NUCLIDE BUILDUP IN OFF-GAS SYSTEM

The OGS in a MSR plays an important role in managing gaseous FPs during reactor operation. Noble gases like xenon and krypton, which are produced during fission, are strong neutron absorbers. If allowed to accumulate in the fuel salt, they can negatively impact the neutron economy, reducing the fission reaction rates. Furthermore, their accumulation increases the pressure within the loop. To mitigate these issues, the OGS is designed to efficiently remove these gases. One common method for this involves bubbling helium through the molten salt (Robertson 1965). Since noble gases like xenon and krypton are insoluble in molten salt, they naturally migrate toward the helium bubbles. These bubbles, now containing FPs, are then separated from the salt and directed to the OGS for further processing.

Another function of the OGS is to contain radioactivity associated with the gaseous FPs. Most of the gases produced during fission are radioactive, and the OGS is designed to safely capture and contain them before further handling. This process typically involves filters or decay tanks that either trap radioactive gases or allow short-lived isotopes to decay over time. For instance, in the conceptual design of the MSBR, the OGS includes a series of holdup systems to manage these gases. Initially, the off-gases are held in a drain tank for about 2 h, after which they move to short holdup charcoal beds for 47 h, followed by long-delay charcoal beds for up to 90 d. This staged process ensures that the radioactive gases have sufficient time to decay before final handling, significantly reducing their radioactivity and the potential risks associated with their disposal (Robertson 1971).

The activity of the OGS in the reference MSR model was analyzed, with results illustrated in Figure 13. In this analysis, a single mixture was used to represent the removal of noble gases from the primary fuel salt to the OGS. No removal path from this mixture to the charcoal beds was considered. Using the ideal gas law, and assuming room temperature and standard pressure, the volume of the gases removed through the OGS after four years was calculated to be ~146.9 m^3. Based on these conditions, the volumetric activity was estimated to reach ~9.013 Ci/cm^3 by the end of the cycle, or after four years of operation.

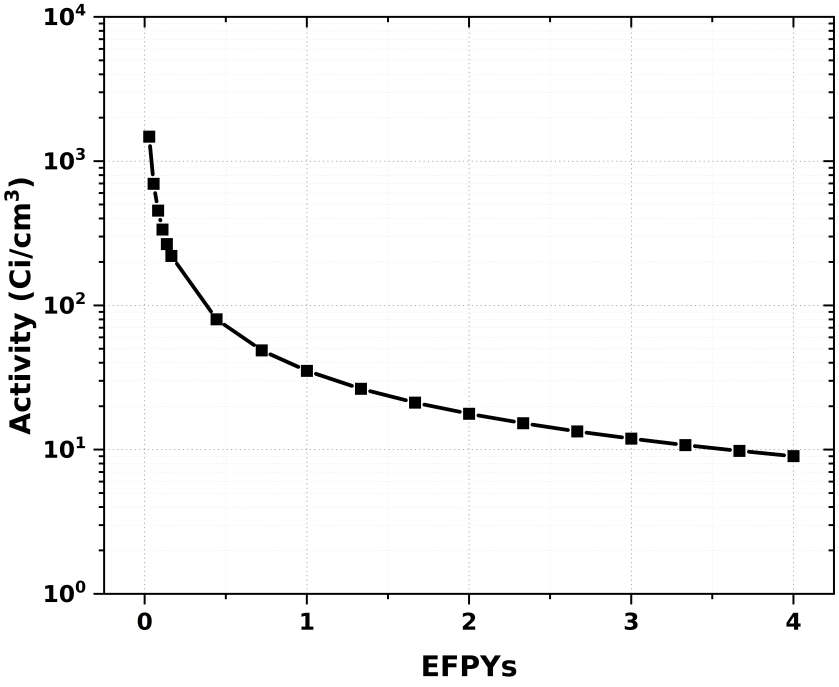

Figure 13. Volumetric activity in the OGS during operation.

This estimate represents an upper bound for the activity within the OGS, as it does not account for removal pathways, which would likely result in lower activity levels. If these removal paths were considered, a portion of the gases would be held in charcoal beds to decay, leading to a reduction in the overall activity within the OGS. The major contributors to the total activity in the OGS during reactor operation are primarily xenon isotopes, as outlined in Table 2. Cesium-138, which is a decay product of ^{138}Xe, is also identified as a significant contributor to the total activity in the OGS. Notably, the radionuclides listed are short-lived, with half-lives ranging from approximately 10 minutes to 5 days.

Table 2. Top contributors to the activity in the OGS during operation

Isotope	Contribution to total activity (%)
^{135}Xe	9.00
^{133}Xe	8.62
^{138}Cs	7.62
^{138}Xe	7.62
^{137}Xe	7.34

The radiotoxic FPs present in the OGS after four years of operation were analyzed. In a study by Thomas and Jerden from 2020, major FPs were identified in terms of their radiotoxicity, drawing on data from a report from the US Environmental Protection Agency (Eckerman, Wolbarst, and Richardson 1988). These isotopes are characterized using three key radiological safety factors: the annual limit on intake (ALI), the derived air concentration (DAC), and the effective dose equivalent conversion factor (Thomas and Jerden 2020; Eckerman, Wolbarst, and Richardson 1988). An ALI represents the maximum amount of a radionuclide that if ingested or inhaled by an individual would result in a committed radiation dose equal to the regulatory dose limit, ensuring that exposure remains within safe levels over a given time period. This metric is crucial for

assessing radiological safety during routine and accidental exposures. The DAC indicates the concentration of a radionuclide in the air that if inhaled continuously over a standard work-year (~2,000 h) would result in an intake equivalent to the ALI. Additionally, the effective dose equivalent conversion factor quantifies the potential damage that a radionuclide can cause to different organs in the body (Eckerman, Wolbarst, and Richardson 1988; Thomas and Jerden 2020).

Table 3 lists the radiotoxic FPs ranked by their dose factor. The table also summarizes radioactivity data such as the half-life and the cumulative yields for thermal neutron fission of ^{235}U, as well as radiotoxicity data including the dose factor, the DAC, and the ALI for both inhalation and ingestion. Additionally, it provides the concentrations of these isotopes after four years of operation in the OGS of the reference MSR model. Although only xenon and krypton were continuously removed from the primary fuel salt to the OGS, 21 other radiotoxic nuclides, excluding xenon and krypton isotopes, were found in the OGS with the concentrations exceeding 1.0×10^{-10} mole, generated primarily from the decay of xenon, krypton, and their daughter isotopes. Collectively, these radiotoxic nuclides contributed ~25.6% of the total activity in the OGS at the end of the four-year operational period.

Table 3. Major radiotoxic FPs (Thomas and Jerden 2020) in the OGS after four years of operation. Missing values in the last column indicate that the concentration is negligible (below 1E-10 moles)

Nuclide	Half-Life (days)	^{235}U Cum. Yield	Dose Factor (mrem/mCi)	DAC (MBq/m^3)	Inhalation ALI (MBq)	Ingestion ALI (MBq)	Activity after 4 years (MBq)
^{135}Cs	8.39E+08	6.54E-02	706.7	2.0E-02	40	30	5.96E+06
^{129}I	5.73E+09	5.43E-03	276.0	1.0E-04	0.3	0.2	
^{90}Sr	1.05E+04	5.78E-02	142.5	3.0E-04	0.7	1	1.26E+11
^{131}I	8.03E+00	2.89E-02	53.3	7.0E-04	2	1	
^{137}Cs	1.10E+04	6.19E-02	50.0	2.0E-03	6	4	3.38E+11
^{106}Ru	3.72E+02	4.02E-03	27.4	1.0E-03	3	7	
^{144}Ce	2.85E+02	5.50E-02	21.0	4.0E-04	0.9	8	2.03E+08
^{115m}Cd	4.46E+01	1.00E-05	16.2	8.0E-04	2	10	
^{125}Sn	9.64E+00	1.60E-04	12.3	1.0E-02	30	10	
^{90}Y	2.67E+00	5.78E-02	10.8	3.0E-03	30	20	1.26E+11
^{129m}Te	3.36E+01	9.02E-04	10.7	1.0E-02	20	20	
^{133}I	8.67E-01	6.70E-02	10.4	4.0E-03	10	5	
^{91}Y	5.85E+01	5.83E-02	9.5	4.0E+00	9,000	20	4.56E+11
^{140}Ba	1.28E+01	6.21E-02	9.5	2.0E-02	50	20	7.84E+11
^{132}Te	3.20E+00	4.29E-02	9.4	4.0E-03	9	8	
^{89}Sr	5.05E+01	4.73E-02	9.3	1.0E-02	30	20	1.96E+12
^{156}Eu	1.52E+01	1.49E-04	9.2	7.0E-03	20	20	
^{79}Se	1.08E+08	4.47E-04	8.7	1.0E-02	30	20	
^{140}La	1.68E+00	6.22E-02	8.4	2.0E-02	50	20	7.84E+11
^{127m}Te	1.09E+02	2.51E-04	8.3	4.0E-03	10	20	
^{111}Ag	7.45E+00	1.74E-04	5.1	2.0E-02	60	30	
^{87}Rb	1.76E+13	2.56E-02	4.9	2.0E-02	60	40	7.56E+01
^{143}Pr	1.36E+01	5.96E-02	4.7	1.0E-02	30	30	3.53E+08
^{93}Y	4.24E-01	6.35E-02	4.6	4.0E-02	100	40	1.28E+10
^{127}Sb	3.85E+00	1.57E-03	4.4	3.0E-02	80	30	
^{147}Nd	1.10E+01	2.25E-02	4.4	1.0E-02	30	40	3.12E+03
^{149}Pm	2.21E+00	1.08E-02	4.0	3.0E-02	70	40	

Table 3. (Continued) Major radiotoxic FPs (Thomas and Jerden 2020) in the OGS after four years of operation

Nuclide	Half-Life (days)	^{235}U Cum. Yield	Dose Factor (mrem/mCi)	DAC (MBq/m^3)	Inhalation ALI (MBq)	Ingestion ALI (MBq)	Activity after 4 years (MBq)
^{95}Zr	6.40E+01	6.50E-02	3.8	2.0E-03	5	50	3.27E+07
^{103}Ru	3.92E+01	3.03E-02	3.0	3.0E-02	60	70	
^{99}Mo	2.75E+00	6.11E-02	3.0	4.0E-02	100	60	2.11E+02
^{141}Ce	3.25E+01	5.85E-02	2.9	1.0E-02	30	60	5.40E+10
^{125}Sb	1.01E+03	3.40E-04	2.8	4.0E-02	90	80	
^{95}Nb	3.50E+01	6.43E-02	2.6	2.0E-02	50	80	3.26E+07
^{91}Sr	4.01E-01	5.83E-02	2.5	9.0E-02	200	80	4.48E+11
^{93}Zr	5.58E+08	6.35E-02	1.7	1.0E-04	0.2	50	2.51E+04
^{155}Eu	1.73E+03	3.21E-04	1.5	1.0E-03	3	100	
^{105}Rh	1.47E+00	9.64E-03	1.5	2.0E-01	400	100	
^{99}Tc	7.71E+07	6.11E-02	1.5	8.0E-02	200	100	2.88E-03
^{119m}Sn	2.93E+02	3.44E-06	1.4	4.0E-02	90	100	
^{117m}Sn	1.36E+01	2.62E-07	1.2	2.0E-02	50	60	
^{147}Pm	9.58E+02	2.25E-02	1.0	2.0E-03	5	200	2.03E+03
^{121}Sn	1.13E+00	1.29E-04	0.9	2.0E-01	600	200	
^{151}Sm	3.29E+04	4.19E-03	0.4	2.0E-03	4	500	
^{107}Pd	2.37E+09	1.46E-03	0.1	3.0E-01	800	1,000	
^{83}Br	1.00E-01	5.36E-03	0.1	1.0E+00	2,000	2,000	
^{99m}Tc	2.50E-01	5.38E-02	0.1	2.0E+00	6,000	3,000	
^{85}Kr	3.93E+03	2.83E-03	N/A	5.0E+00	N/A	N/A	3.49E+10
^{85m}Kr	1.87E-01	1.29E-02	N/A	8.0E-01	N/A	N/A	6.63E+11
^{133}Xe	5.24E+00	6.70E-02	N/A	4.0E+00	N/A	N/A	4.65E+12
^{135}Xe	3.81E-01	6.54E-02	N/A	5.0E-01	N/A	N/A	4.74E+12

SCALE/SAMPLER was employed to perform an uncertainty quantification for the radiotoxic nuclides identified in the OGS of the reference MSR model. This analysis involved 500 SCALE/TRITON depletion cases, each using a 2D quarter axial core slice model to reduce the computing time while maintaining the neutron spectrum of the 3D core. Additionally, the neutron transport calculations were performed in multigroup mode using a 56 energy-group library instead of the more computationally expensive continuous-energy mode to further reduce the computing time. The multigroup calculations incorporated appropriately self-shielded cross sections, in which they showed small but acceptable differences in both the multiplication factor (less than 50 pcm) and the neutron spectrum when compared with the reference continuous-energy calculations.

The uncertainty analyses accounted for several important operational parameters that could affect the production of FPs and, subsequently, the concentrations of radiotoxic nuclides in the OGS. The perturbed parameters included fuel temperature, moderator temperature, FP removal rates, and operating power, as summarized in Table 4. The uncertainties associated with these operational parameters were assumed or arbitrarily defined, serving solely to establish correlations. Fuel temperature and moderator temperature influence the neutron spectrum and reaction rates within the reactor. The FP removal rate, particularly relevant to noble gases such as xenon and krypton, affects the accumulation of these radiotoxic nuclides in the OGS. Finally, operating power, which dictates the rate of fuel consumption, also plays a role in determining the

production of FPs. Figures 14–18 illustrate the concentration distributions of these radiotoxic nuclides in response to the perturbation of the operating parameters, where the focused parameter and other parameters are allowed to vary within their respective variances.

The results of the uncertainty analyses are presented through a Pearson correlation matrix, which highlights the relationships between key operational parameters and the buildup of radiotoxic nuclides in the OGS, as depicted in Figure 19. The Pearson correlation coefficient, ranging from -1 to +1, quantifies these relationship. A positive coefficient reflects a direct linear relationship, where both variables increase together, while a negative coefficient indicates an inverse linear relationship, where one variable decreases as the other increases. A coefficient of 0 suggests no linear correlation. The magnitude of the coefficient indicates the strength of the relationship, with values closer to ±1 representing a stronger linear relationship. The analysis reveals that two major parameters—the removal rate of gaseous fission products from the primary salt to the OGS and the operating power—are the primary drivers influencing the accumulation of these nuclides.

Table 4. Operating parameters uncertainty

Parameter	Distribution	Nominal	Relative Standard Deviation (%)
Fuel temperature	Uniform	909.04 K	10
Moderator temperature	Uniform	909.04 K	10
Noble metals removal rate	Uniform	3.333E-02	50
Noble gases removal rate	Uniform	3.333E-02	50
Operating power	Uniform	100%	10

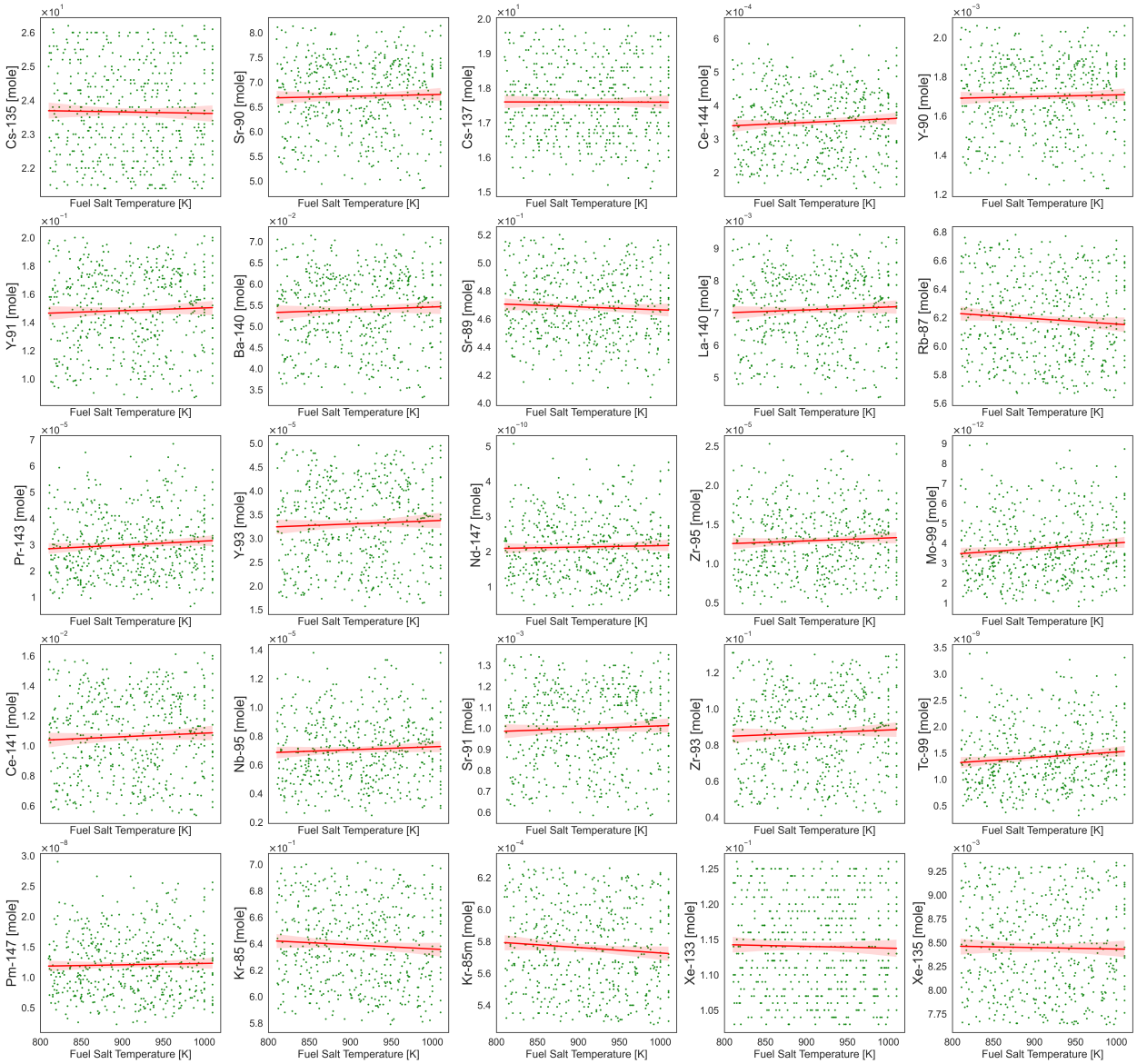

Figure 14. Sensitivity of selected nuclide concentrations in OGS to fuel temperature.

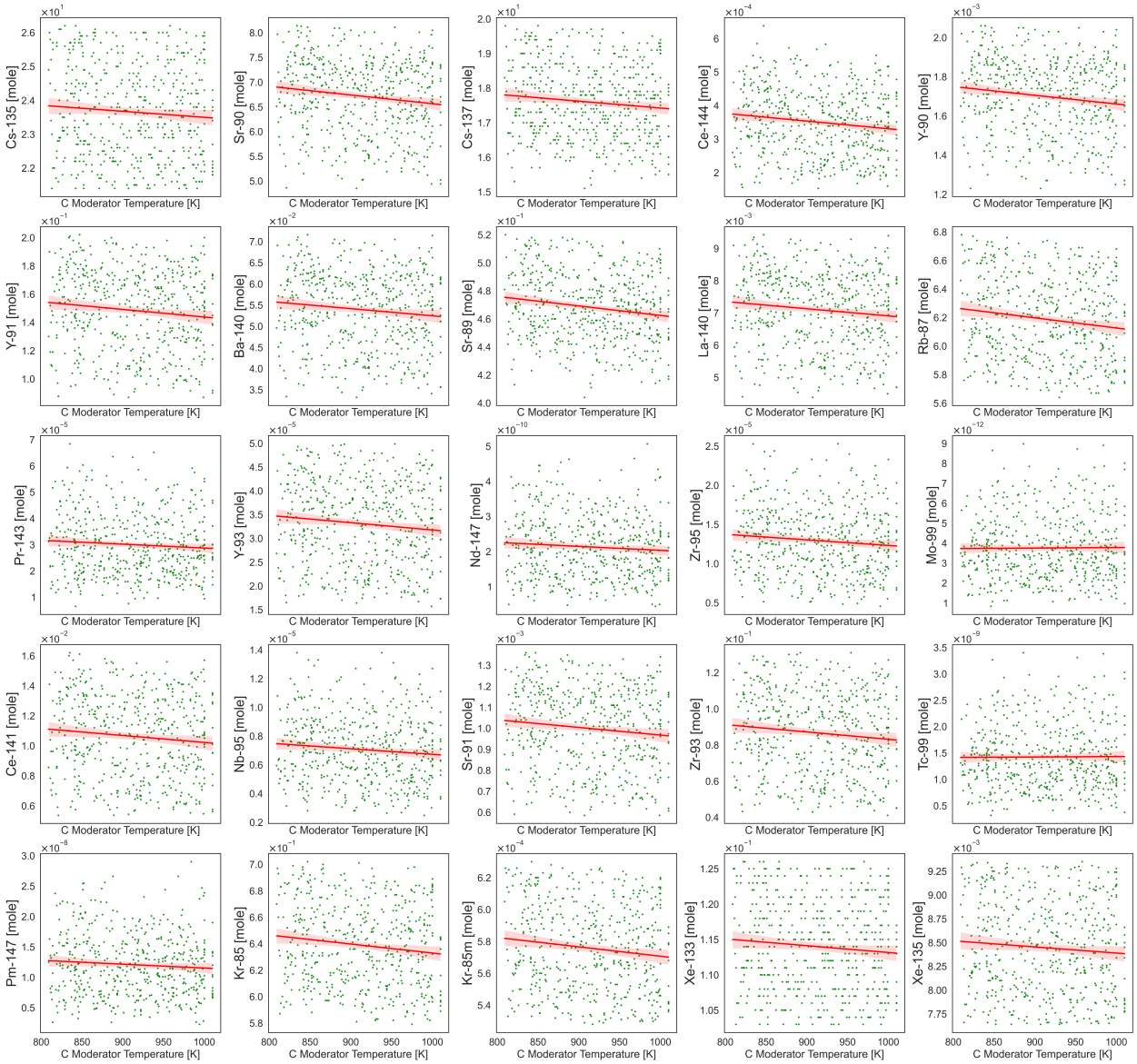

Figure 15. Sensitivity of selected nuclide concentrations in OGS to moderator temperature.

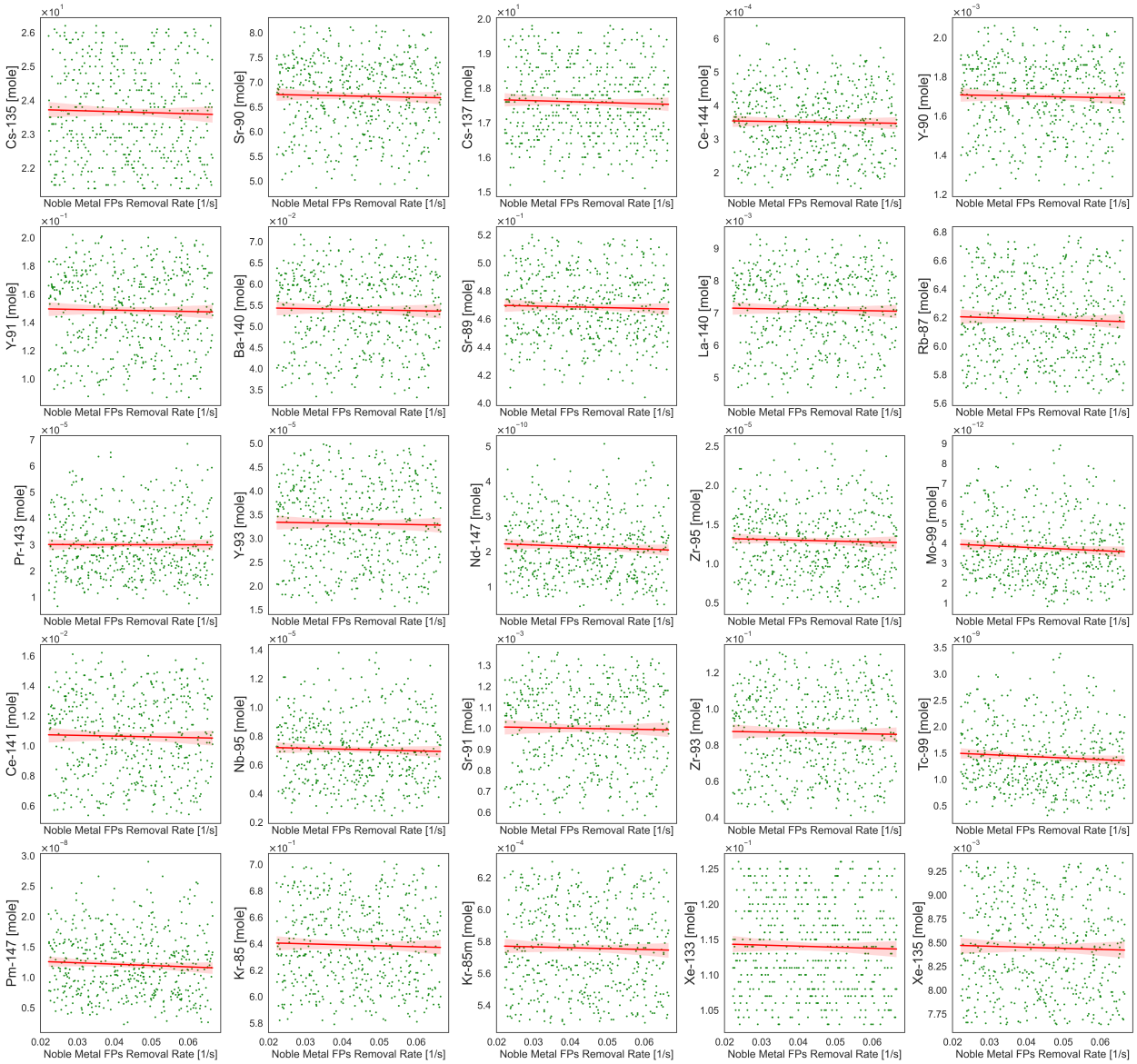

Figure 16. Sensitivity of selected nuclide concentrations in OGS to noble metal removal rates.

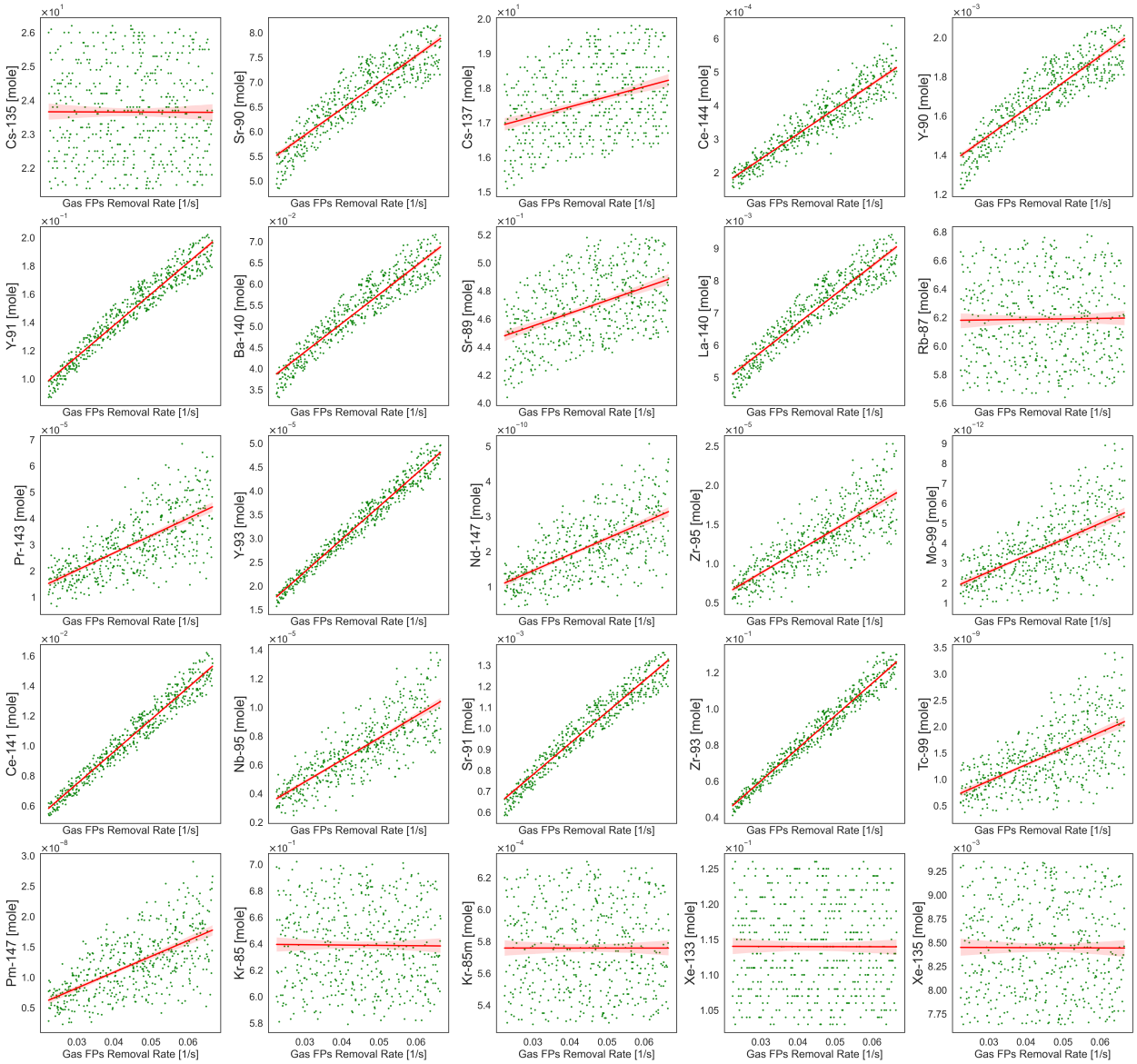

Figure 17. Sensitivity of selected nuclide concentrations in OGS to noble gas removal rates.

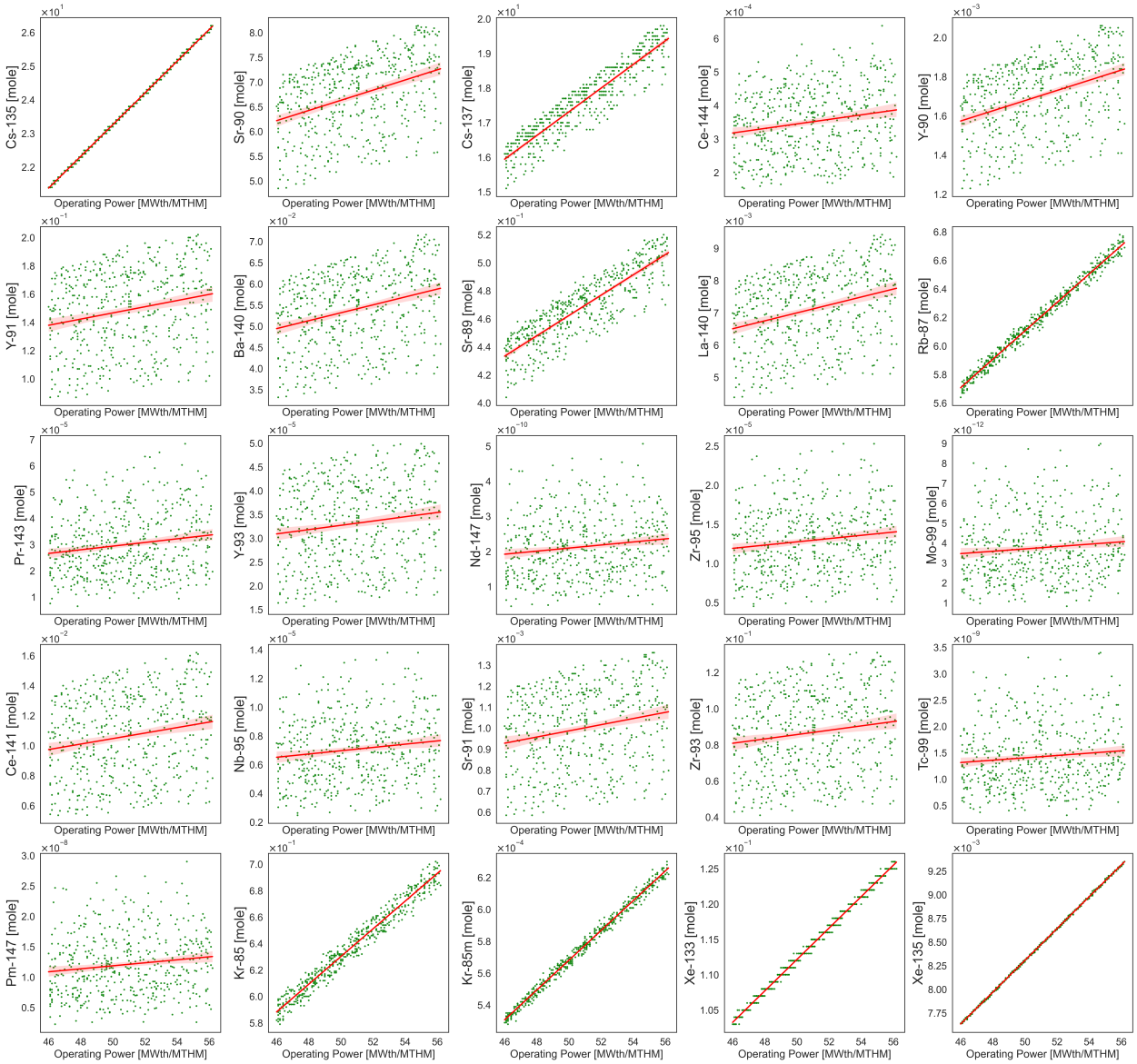

Figure 18. Sensitivity of selected nuclide concentrations in the OGS to operating power.

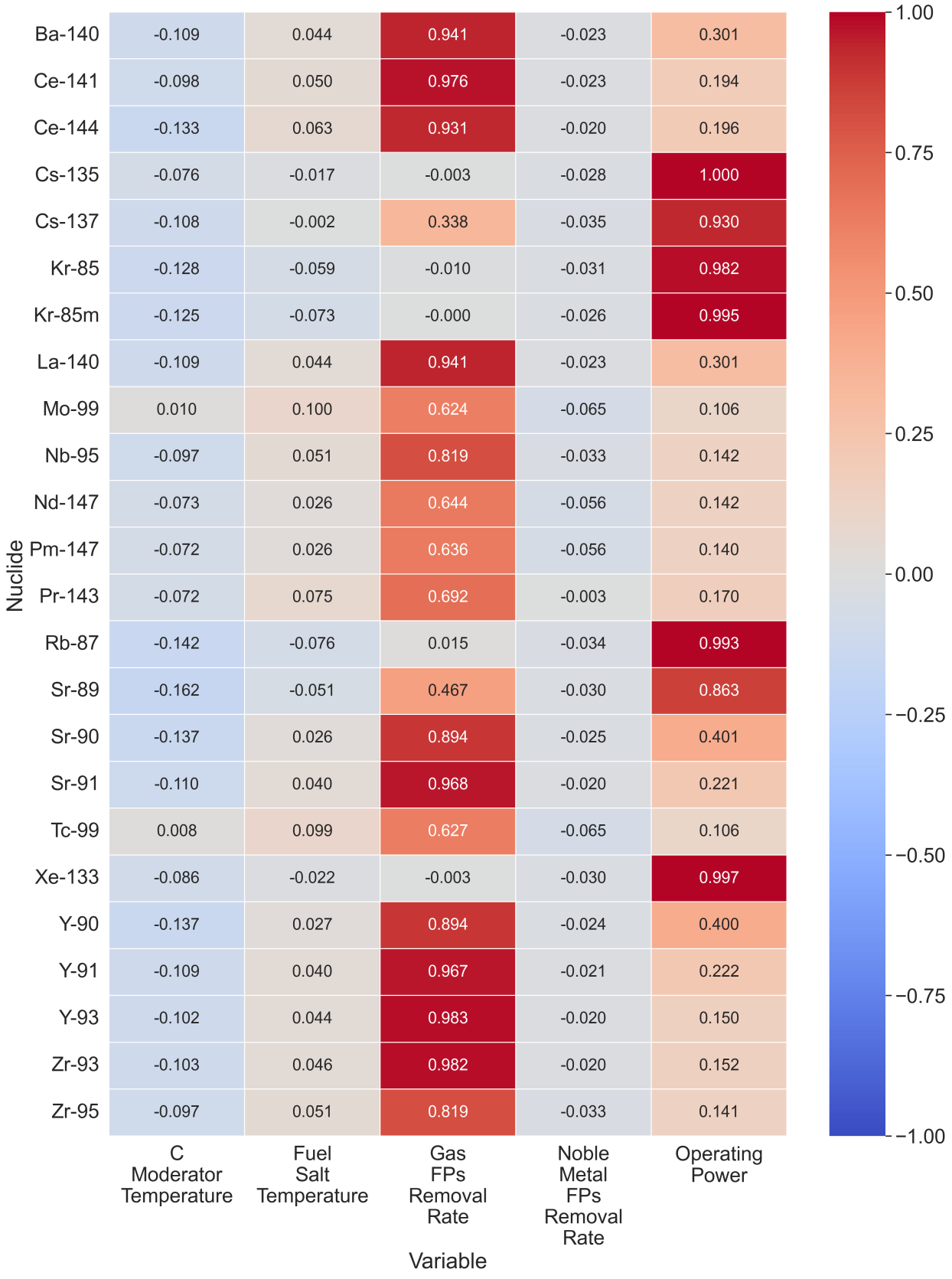

Figure 19. Correlation between nuclide concentrations in the OGS and operating parameters.

Nuclides that exhibit a strong positive correlation with operating power are primarily those that are produced directly as FPs and are subsequently transferred to the OGS, such as xenon and krypton. These isotopes are generated in significant quantities during the fission process, and higher operating power results in increased fission rates, directly affecting the rate at which these gaseous FPs accumulate in the OGS. Additionally, nuclides with very long half-lives, such as ^{135}Cs, ^{137}Cs, and ^{87}Rb, also tend to show high correlation with operating power, as their slow decay rates allow them to persist and accumulate over extended periods of reactor operation.

On the other hand, nuclides that strongly correlate with the noble gas removal rate are typically decay products of the removed gaseous FPs xenon and krypton. As these noble gases are removed from the primary fuel salt and transferred to the OGS, their radioactive decay leads to the production of secondary isotopes. The removal rate thus plays a key role in controlling the concentration of these decay products, which can significantly contribute to the overall radiotoxicity within the OGS.

4.4 OPERATIONAL DOSE RATE

The operational dose rate was calculated after four years of reactor operation (i.e., using the reactor's fuel salt inventory after four years as the radiation source). For this calculation, a simplified model of the reference MSR plant was developed, as illustrated in Figure 20. This simplified plant model focused on the primary structure of the reactor building, excluding components such as heat exchangers, pumps, and pipes to reduce model complexity. The building's walls were assumed to be constructed from ordinary concrete, with a thickness of ~2.5 m for the reactor cell and 0.9 m for the walls of the other parts of the building (Davidson et al. 2021). The walls were further reinforced with a 1.27 cm thick carbon steel shell (Robertson 1971).

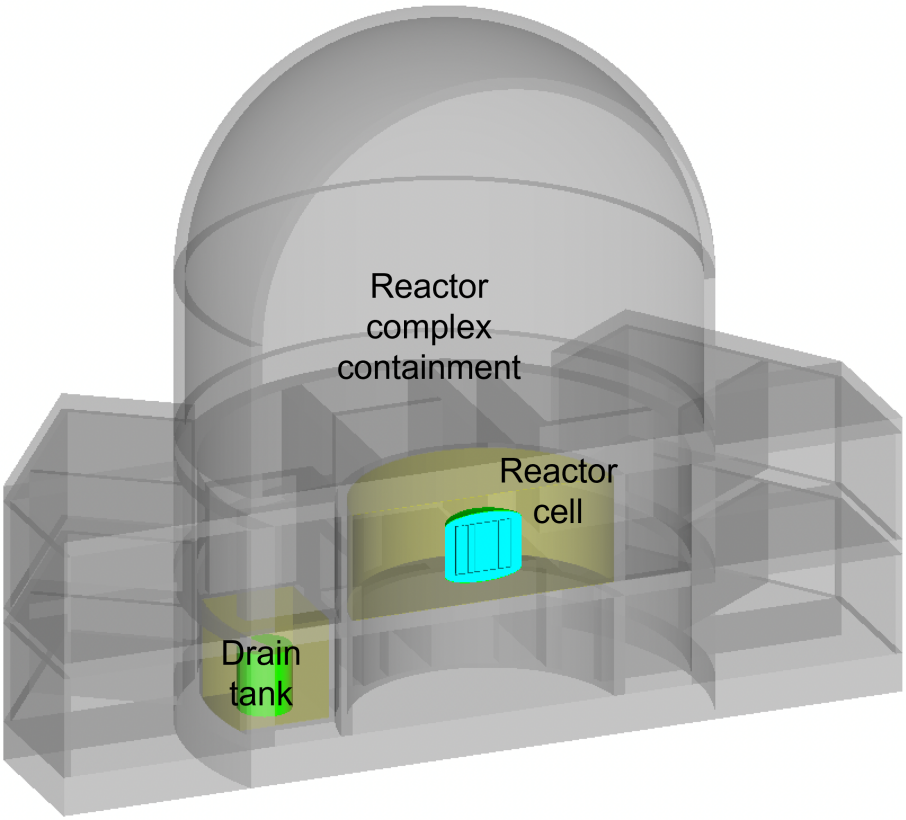

Figure 20. Reference MSR plant model for dose rate calculation.

To perform the dose rate calculations, the spatial and energy distributions of fission neutrons were obtained from a SCALE/CSAS calculation of the reference MSR core. The fission source was generated using a mesh tally with $51 \times 51 \times 70$ voxels, along with a 200-group neutron energy structure, as shown in Figure 21. The total strength of this source was calculated to be $\sim 1.85 \times 10^{20}$ neutrons/s. This value was derived using the total average number of neutrons per fission, the total reactor power, and ~200 MeV energy per fission.

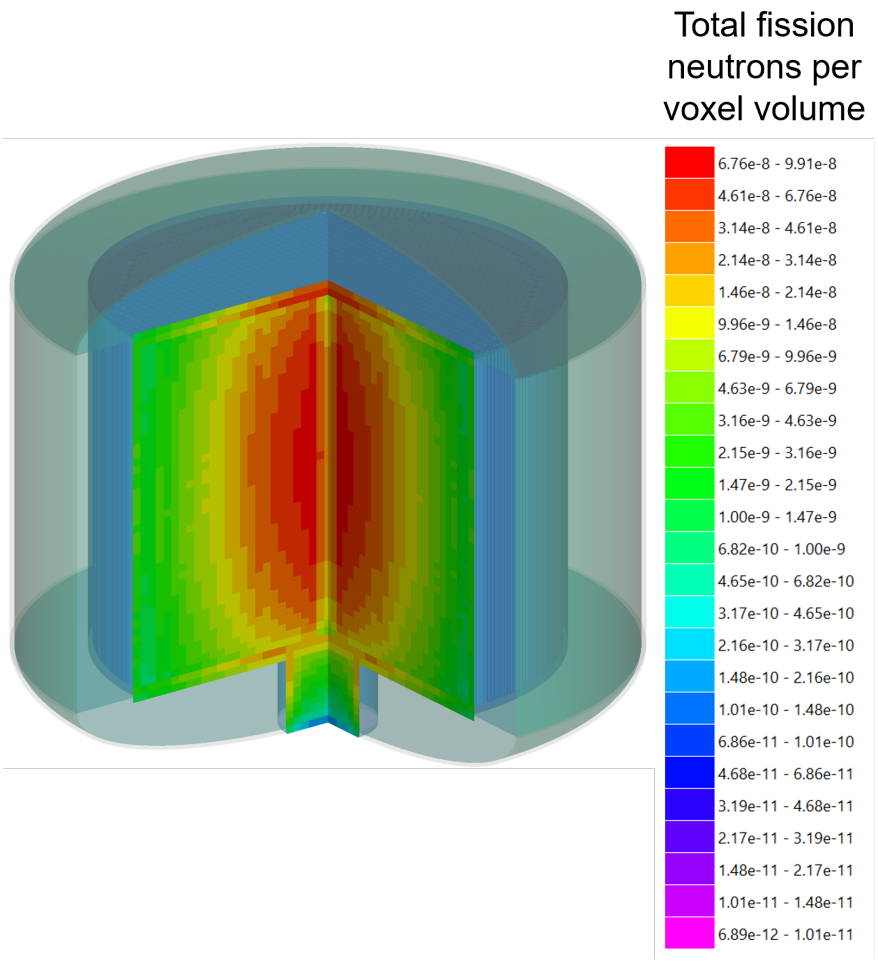

Figure 21. Neutron fission source spatial distribution.

In the dose calculation carried out using SCALE/MAVRIC, the fission prompt gamma source was generated based on the prompt fission neutrons. Note that radiation sources from FP decay and activation were not included in this calculation, as their contribution to the total dose is typically much lower than that of prompt fission neutrons and gamma radiation produced within the core.

The dose rates in both the reactor cell and the surrounding reactor complex region were evaluated, with results illustrated in Figure 22, showing the total dose and the neutron dose. From these graphs, it is evident that gamma radiation dominated the total dose rate. Another interesting observation is that the model had an effective shielding design, providing adequate shielding based on the specific needs of each area. For instance, in the reactor cell region, the total dose rate exceeded 1.5×10^6 rem/h, which is consistent with the expected high radiation levels near the active core. However, the dose rate near the new core replacement region was reduced to $\sim 1.5 \times 10^{-1}$ rem/h, protecting the new core unit. In contrast, the spent core storage area, where used reactor cores are kept, exhibited a higher dose rate of $\sim 2.0 \times 10^3$ rem/h. Although the

presence of personnel within the reactor complex region during operation is not expected, for reference, the occupational annual dose limit for adults specified in Title 10 of the Code of Federal Regulations, Part 20.1201, is a total effective dose equivalent of 5,000 mrem (50 mSv).

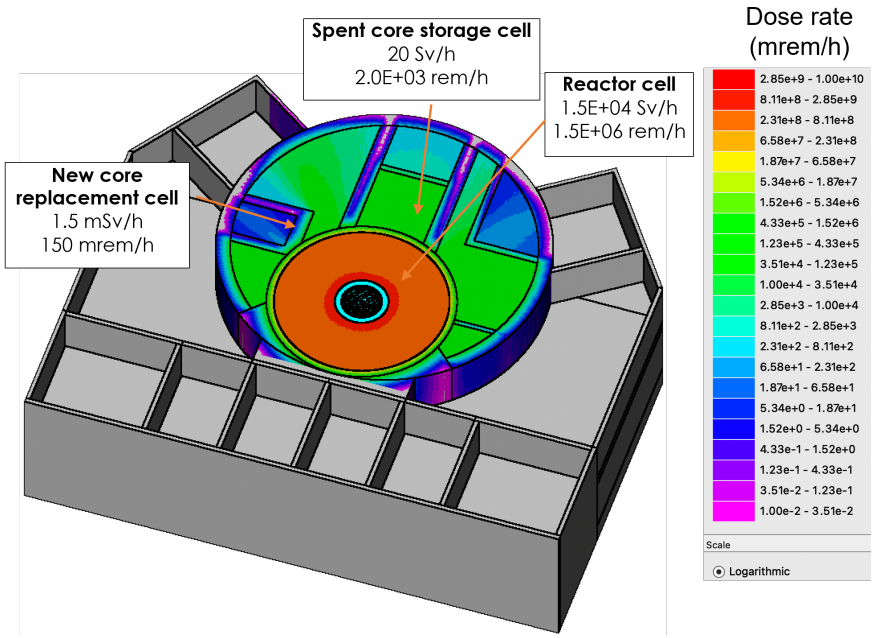

(a) Total dose rate map

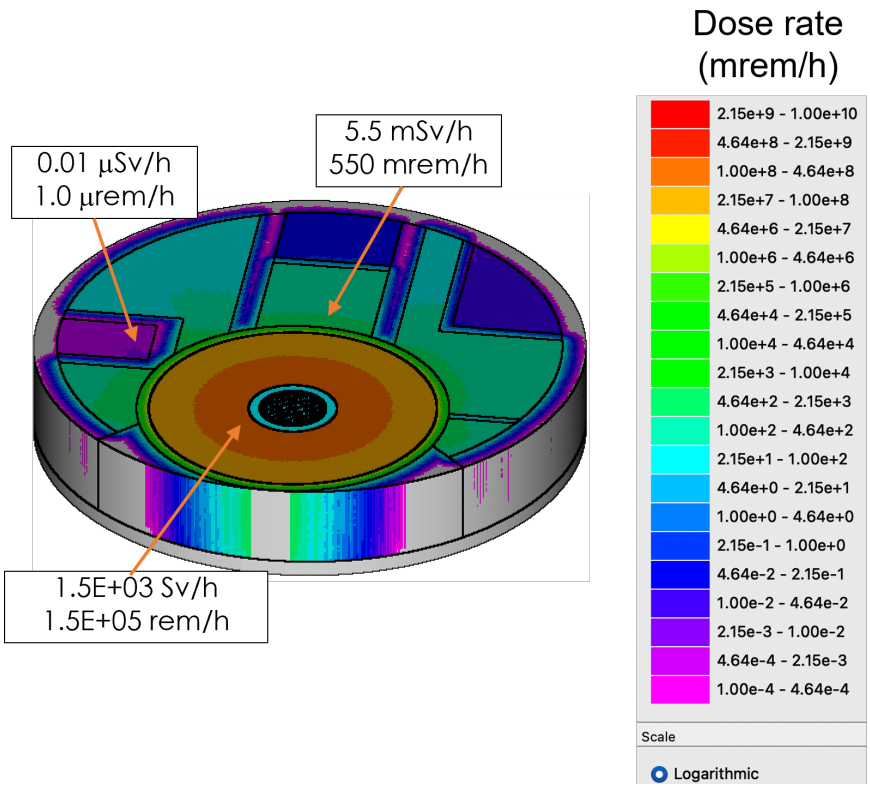

(b) Neutron dose rate map

Figure 22. Total and neutron dose rate maps in the reactor complex cell.

5. SCENARIO 3: FAILURE IN HEAT REMOVAL OF DRAIN TANK

This scenario examines the consequences of a failure in the heat removal system of the drain tank. In the legacy MSBR conceptual design report (Robertson 1971), the primary function of the drain tank is to safely contain and cool the fuel salt in both accidental and intentional situations, such as reactor shutdowns or emergencies. The drain tank is also designed to serve as a 2-h holdup volume for gaseous FPs during normal operation. Its location, as depicted in Figure 23, is at a lower elevation than the reactor area, which helps facilitate the natural draining of fuel salt in the event of an emergency. The drain tank is equipped with its own cooling system to manage decay heat effectively.

In this analysis, a complete failure of the cooling system was assumed after the fuel salt from the core was completely drained into the tank, leading to a loss of heat removal capacity. The decay heat produced by the fuel salt was evaluated to assess the potential heat generated in the absence of active cooling. This decay heat data was subsequently utilized by the SNL team in MELCOR simulations to model the loss of heat removal in the drain tank. Additionally, radiation shielding calculations were performed to assess the radiation levels using the collected fuel salt as the source term. The fuel inventory from Scenario 2 was used as the radiation source for these calculations.

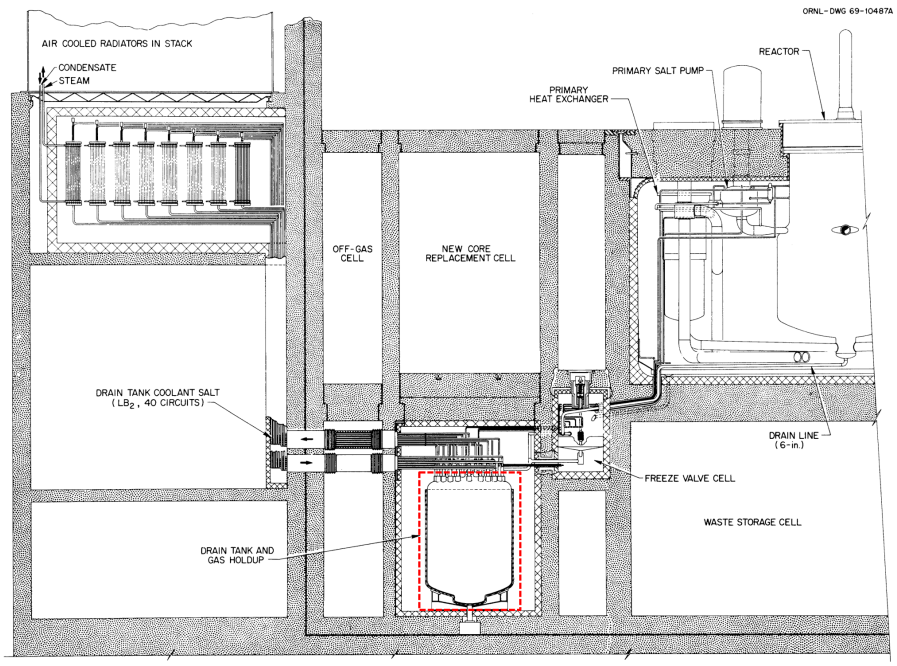

Figure 23. Location of the drain tank (Robertson 1971).

5.1 DECAY HEAT OF DRAIN TANK

The decay heat generated in the drain tank is influenced primarily by the quantity and type of FPs and actinides present in the irradiated fuel. To provide a clearer understanding, it is helpful to compare the composition of fresh and spent fuel salt from the reference MSR model with that of a pressurized water reactor (PWR) right after discharge. Figure 24 illustrates the relative weight fractions of FPs, actinides (ACs), and light elements (LTs)—nuclides with atomic numbers below 90 that are not fission or decay products such as salt components—in the MSR at the beginning and end of the 4 EFPY cycle alongside the

inventory of a PWR. The spent fuel composition of a PWR was obtained from a 3,000 MWth PWR with an initial enrichment of 4.2 wt% and achieving a burnup of 50 GWd/metric ton initial heavy metal (MTIHM) that was previously generated for another non-LWR assessment effort (Hartanto, Radulescu, et al. 2024). This PWR spent fuel composition is used for comparison throughout the remainder of this section.

One key observation is that MSR fuel salt contains more than 60% LTs, such as lithium and beryllium, which can become activated during reactor operation. These activated light elements contribute ~1.91% to the decay heat and ~0.79% to the overall activity in MSR spent fuel salt. In contrast, the contribution of LTs, primarily oxygen, in PWR fuel is negligible. Another noteworthy observation is the significantly lower FP content in the MSR spent fuel salt, which contains only ~0.32 wt% FPs. This low fraction is because of the continuous removal of FPs during operation, which limits their accumulation. Despite this low fraction, FPs in MSR spent fuel salt contribute to ~89.15% of its decay heat and ~63.65% of the total activity. In comparison, PWR spent fuel contains ~4.5% FPs, which contribute to ~94.37% of the decay heat and 78.39% of the total activity.

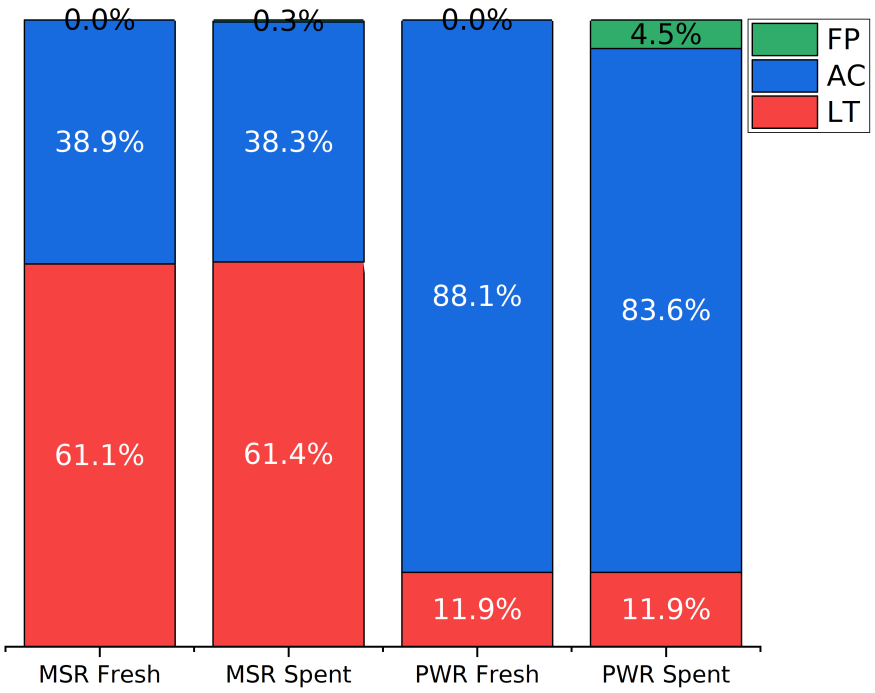

Figure 24. Fuel inventory (relative weight fractions) compared between fresh and spent fuels of the MSR and a PWR.

The decay heat of the MSR fuel salt in the drain tank as function of cooling time is illustrated in Figure 25. For comparison, the decay heat of PWR spent fuel is also included in the figure. The initial decay heat for the reference MSR model was ~4% of the operating power, whereas for the PWR spent fuel, it was ~6% of the operating power. One key factor contributing to the lower fraction of decay heat in the MSR is the lower burnup achieved due to its continuous makeup fuel feed. After four EFPY, the estimated burnup for the MSR is about 16.59 MWd/tHM, which is roughtly three times lower than that of the PWR. Furthermore,the continuous removal of FPs such as xenon, krypton, and noble metals from the primary fuel salt during operation also reduces the accumulation of isotopes that contribute to the decay heat in conventional reactors like the PWR. The major contributors to the decay at shutdown and after five years of cooling time are listed in Table 5. A similar trend is also observed in the activity as a function of cooling time, shown in Figure 26, in which the activity over time for the MSR is lower than that of the PWR.

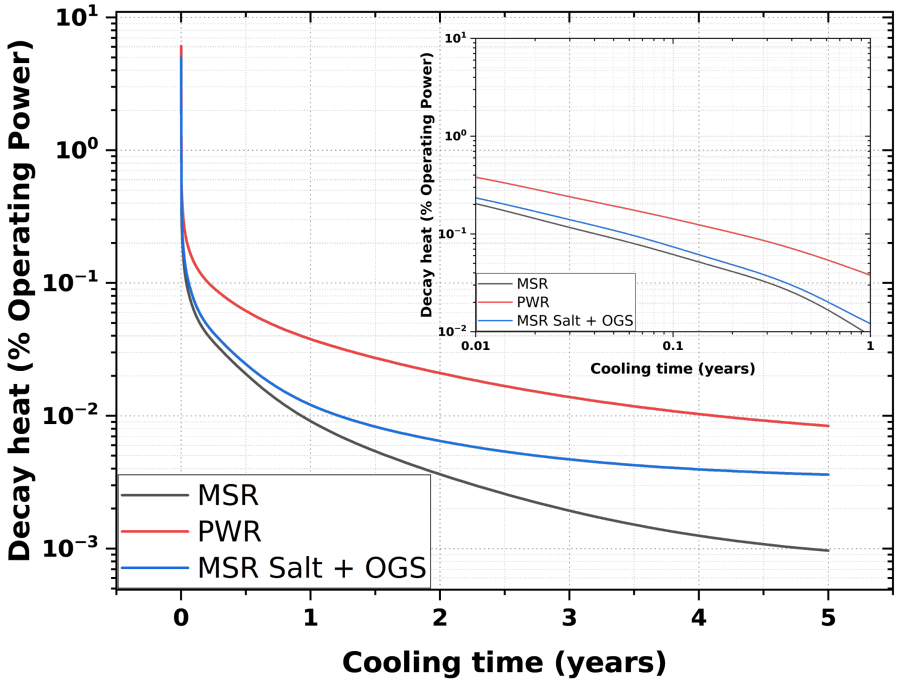

Figure 25. Comparison of decay heat as function of cooling time between MSR spent fuel salt in the drain tank and PWR spent fuel. The decay heat after a short cooling period is shown in the snapshot on a log scale to facilitate easy comparison.

Table 5. Top five contributors of decay heat in the MSR and PWR

Shutdown		After Five Years of Cooling	
MSR	PWR	MSR	PWR
^{239}U (4.67%)	^{239}U (2.73%)	^{90}Y (23.70%)	^{134}Cs (18.78%)
^{239}Np (4.06%)	^{239}Np (2.39%)	^{144}Pr (17.48%)	^{90}Y (18.54%)
^{144}La (2.21%)	^{134}I (1.89%)	^{244}Cm (15.61%)	^{137m}Ba (18.38%)
^{100}Nb (2.01%)	^{138}Cs (1.76%)	^{238}Pu (9.12%)	^{244}Cm (8.37%)
^{92}Rb (1.96%)	^{104}Tc (1.64%)	^{241}Am (7.35%)	^{106}Rh (7.80%)

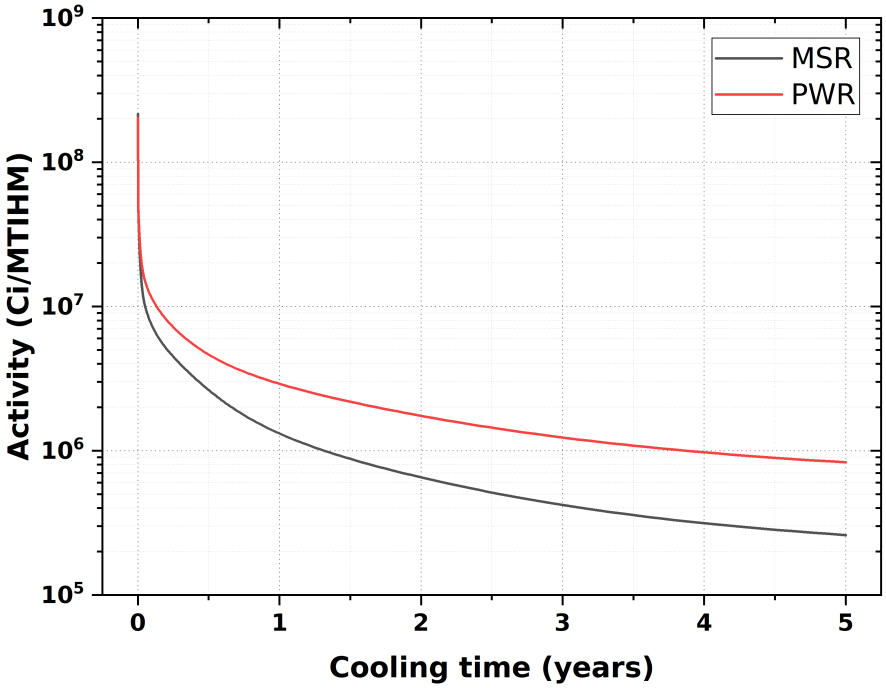

Figure 26. Comparison of activity per MTIHM as a function of cooling time between MSR spent fuel salt in the drain tank and PWR spent fuel.

5.2 DRAIN TANK DOSE RATE

The shielding calculation was conducted to determine the spatial distribution of the dose rate in the air region outside the reactor building, produced by the spent fuel salt contained within the drain tank. The radiation source terms were derived from the discharged fuel salt after four years of operation. These source terms are comparable to those of a PWR spent fuel assembly with a burnup value of 50 GWd/MTIHM. A comparison of their photon and neutron spectra are provided in Figure 27.

The total photon and neutron source intensities at fuel discharge for both reactors are summarized in Table 6. The gamma sources considered in the analysis include radiation from the decay of fission products, actinides, and activation products, as well as Bremsstrahlung radiation. The total gamma source strength per MTIHM for both reactors is quite similar. However, note that a typical 3,000 MWth PWR core contains ~89 MTIHM, whereas the reference MSR contains ~44 MTIHM in its primary loop. This results in a lower overall mass of heavy metals in the MSR compared with the PWR, which affects the total source strength for each reactor when considering the source terms in the entire core.

Meanwhile, the neutron sources in the discharged fuel of both the MSR and the PWR are dominated by delayed neutrons emitted from the decay of FPs. Furthermore, it is interesting to note that neutron sources from (α, n) reactions in the MSR could be ~250 times higher than those in the PWR. This significant difference is primarily because of the presence of beryllium and lithium in the MSR fuel salt, which have higher neutron yields from (α, n) reactions (i.e., 5.010×10^{10} neutrons per second from ^{9}Be and 3.409×10^{9} neutrons per second from ^{7}Li). This represents a unique characteristic of the neutron sources from the discharged MSR fuel salt.

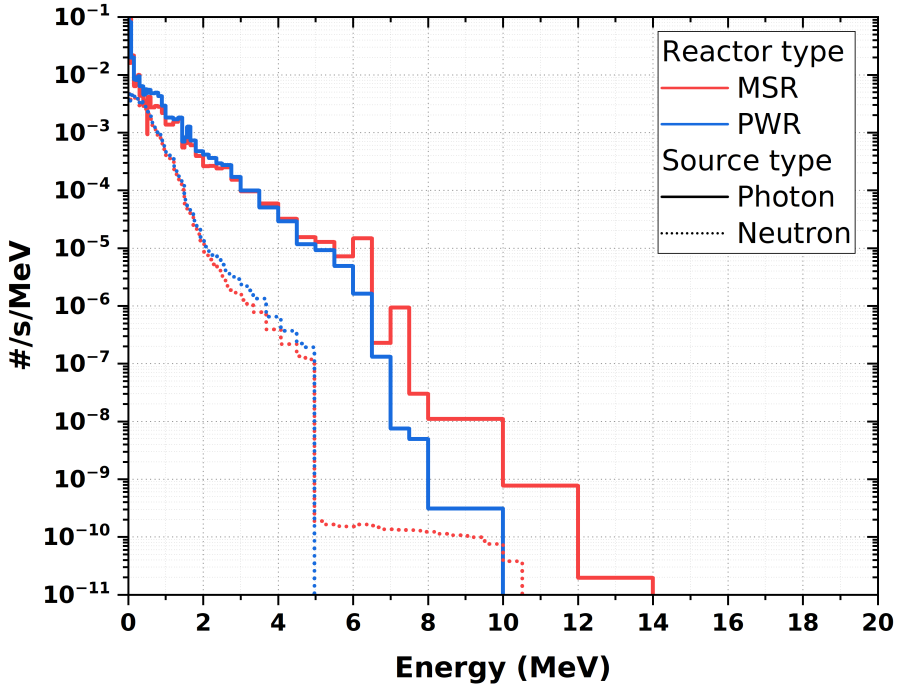

Figure 27. Comparison of photon and neutron spectra between MSR spent fuel salt and PWR spent fuel at fuel discharge.

Table 6. Photon and neutron source intensities of MSRs and PWRs at fuel discharge

Reactor	Photon/s/MTIHM	Neutron/s/MTIHM			
		Delayed Neutrons	(α,n) Reactions	Spontaneous Fission	Total
MSR	1.3690E+19	2.1638E+16	2.9545E+10	5.9075E+08	2.1638E+16
PWR	1.3879E+19	1.4100E+16	1.1928E+08	1.6768E+09	1.4100E+16

A color-coded 3D dose rate map for the air region outside the building is presented in Figure 28, where the tally mesh voxel size is $30 \times 30 \times 30$ cm. The results show very low external dose rate values compared with the dose rate at the drain tank, demonstrating the effectiveness of the MSR building's design in shielding radiation. The calculated maximum external dose rate is ~30 μSv/h (3 mrem/h) with a relative error of 1.5%. Furthermore, the neutron dose rate was about five orders of magnitude lower than the gamma dose rate, indicating that the concrete walls provide excellent neutron attenuation.

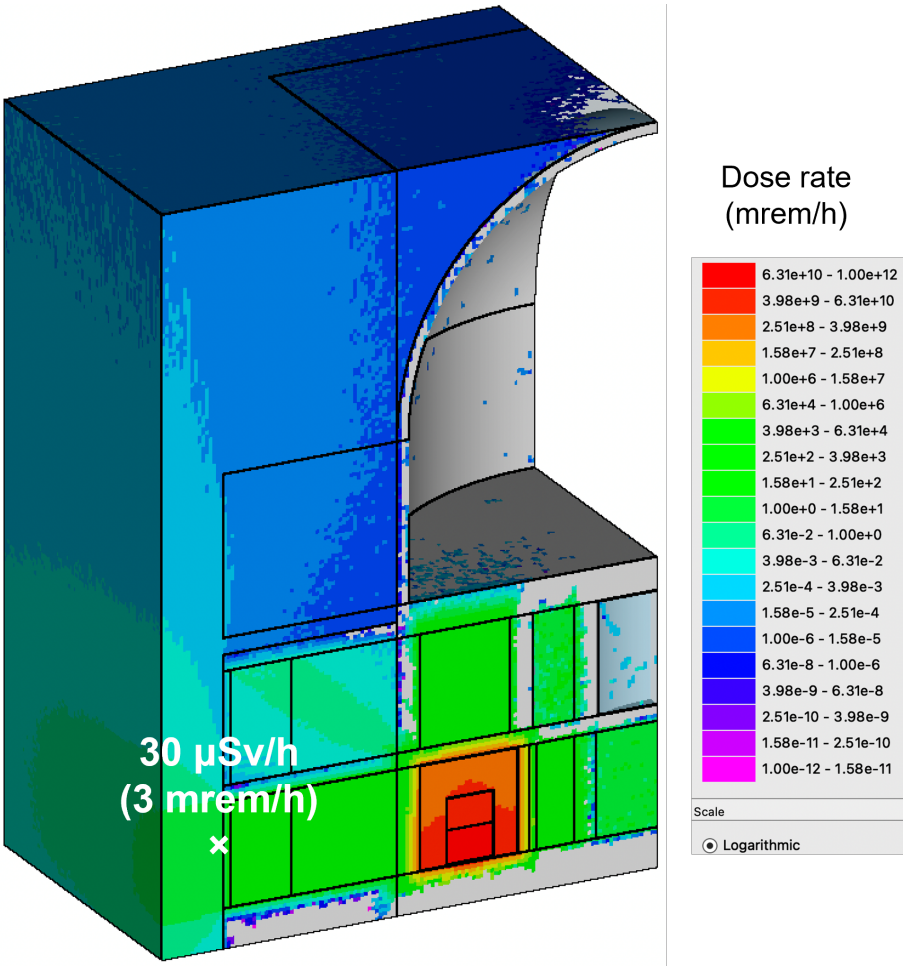

Figure 28. Dose rate map outside of the building from the spent fuel salt in the drain tank.

6. CONCLUSIONS

The extensive capabilities of the SCALE code system in simulating various stages of the MSR fuel cycle have been demonstrated in support of the NRC non-LWR fuel cycle demonstration project. The MSBR, which was design to operate at 2,250 MWth (1,000 MWe), was selected as the reference design since its power range is closer to that anticipated for future commercial MSRs. The original thorium-based fuel salt was replaced with a ^{235}U-enriched fuel salt to reflect anticipated future MSR concepts. Three accident scenarios were explored to demonstrate the code capability, irrespective of the probability of occurrence.

In the first scenario, criticality safety of the fresh fuel salt container was assessed using SCALE/CSAS-Shift and SCALE/SAMPLER, focusing on parameters such as ^{235}U enrichment, UF_4 molar fraction, temperature, and vessel radius. The results highlighted the excellent criticality safety margins of the MSRE fresh fuel salt containers to handle the current salt composition, although criticality safety limits were shown to be exceeded when enrichment levels surpassed 14 wt%. Given that the initial enrichment of the fresh fuel was ~2.3 wt%, there is significant flexibility to adjust vessel dimensions within reasonable limits while maintaining criticality safety. Note that because of the absence of publicly available information, the analyzed fresh fuel salt containers were those used in the MSRE and are not necessarily the ones that will be used in future commercial reactors.

In the second scenario, a release of FPs was modeled to occur after four years of continuous reactor operation. The results showed that the accumulation of tritium within the primary fuel salt after four years of operation was estimated to be ~147 g, corresponding to a volumetric activity of ~38 Ci/L of fuel salt. The behavior of radiotoxic FPs within the OGS was also analyzed. Although only xenon and krypton were continuously removed from the primary fuel salt to the OGS, 21 other radiotoxic nuclides, excluding xenon and krypton isotopes, were found in the OGS with non-negligible concentrations. Collectively, these radiotoxic nuclides contributed ~25.6% of the total activity in the OGS at the end of the four-year operational period. An uncertainty analysis revealed that two major parameters—the removal rate of gaseous fission products from the primary salt to the OGS and the operating power—were the primary drivers influencing the accumulation of these radiotoxic nuclides in the OGS. Accurate determination of this removal rate is important to reduce uncertainties in radiotoxic nuclide concentrations. Radiation shielding calculations were also performed in this scenario within the reactor cell complex. The results showed that gamma radiation dominated the total dose rate and that the plant had an effective shielding design, providing adequate shielding based on the specific needs of each area.

The final scenario investigated the consequences of a failure in the heat removal system of the drain tank. The results showed that the initial decay heat for the reference MSR model was ~4% of the operating power, lower than 6% observed in the PWR spent fuel. The factor contributing to the lower fraction of decay heat in the MSR was its lower burnup, combined with the continuous removal of FPs from the primary fuel salt during operation. Interestingly, neutron sources from (α, n) reactions in the MSR could be ~250 times higher than those in the PWR because of the high neutron yields from (α, n) of beryllium and lithium. Additionally, the shielding calculation confirmed the effectiveness of the MSR building's design in shielding radiation to attenuate the dose from the drain tank to the region outside the reactor building.

Overall, this study has effectively demonstrated the diverse capabilities of the SCALE code system, including fuel inventory calculations that accounted for FP removal and feed addition, as well as analyses of decay heat, activity, shielding, radiation dose, and criticality of the MSR nuclear fuel cycle through the three selected scenarios. To improve the user experience and capability to simulate a MSR, several future enhancements are planned for the SCALE code. These are mainly focused on additional capabilities in TRITON: (1) permit total reactor power or neutron flux as input parameter (in addition to only permitting

specific power), (2) handle actual fuel masses without normalization to 1 MTIHM, (3) allow fuel salt mass and volume changes in depletion calculations with continuous feed, and (4) enable a simple delayed neutron precursor drift model. Furthermore, the impact of depletion simulation using the balance tank approach will be assessed after SCALE/TRITON has been extended to consider increasing fuel salt mass and volume.

7. REFERENCES

Bostelmann, F., C. Celik, R. F. Kile, and W. A. Wieselquist. 2022. *SCALE Analysis of a Fluoride Salt-Cooled High-Temperature Reactor in Support of Severe Accident Analysis.* Technical report ORNL/TM-2021/2273. Oak Ridge, TN: Oak Ridge National Laboratory. https://doi.org/10.2172/1854475.

Bostelmann, F., E. E. Davidson, W. A. Wieselquist, D. Luxat, K. C. Wagner, and L. I. Albright. 2023. *Non-LWR Fuel Cycle Scenarios for SCALE and MELCOR Modeling Capability Demonstration.* Technical report ORNL/TM-2023/2954. Oak Ridge, TN: Oak Ridge National Laboratory. https://doi.org/10.2172/2251628.

Bostelmann, F., S. E. Skutnik, A. Shaw, D. Hartanto, and W. A. Wieselquist. 2024. *SCALE 6.3 Modeling Strategies for Reactivity, Nuclide Inventory, and Decay Heat of Non-LWRs.* Technical report ORNL/TM-2024/3213. Oak Ridge, TN: Oak Ridge National Laboratory. https://doi.org/10.2172/2351061.

Chadwick, M.B., M. Herman, P. Obložinský, M.E. Dunn, Y. Danon, A.C. Kahler, D.L. Smith, et al. 2011. "ENDF/B-VII.1 Nuclear Data for Science and Technology: Cross Sections, Covariances, Fission Product Yields and Decay Data." *Nuclear Data Sheets* 112 (12): 2887–2996. https://doi.org/10.1016/j.nds.2011.11.002.

Davidson, E. E., G. Radulescu, K. Smith, J. Yang, S. Wilson, and B. R. Betzler. 2021. "Reactor cell neutron dose for the molten salt breeder reactor conceptual design." *Nuclear Engineering and Design* 383:111381. https://doi.org/10.1016/j.nucengdes.2021.111381.

De Hart, M. D., and S. M. Bowman. 2011. "Reactor Physics Methods and Analysis Capabilities in SCALE." *Nuclear Technology* 174 (2): 196–213. https://doi.org/10.13182/NT174-196.

Dolan, K., G. Zheng, K. Sun, D. Carpenter, and L. Hu. 2021. "Tritium generation, release, and retention from in-core fluoride salt irradiations." *Progress in Nuclear Energy* 131:103576. https://doi.org/10.1016/j.pnucene.2020.103576.

Eckerman, K. F., A. B. Wolbarst, and A C.B. Richardson. 1988. "Limiting Values of Radionuclide Intake and Air Concentration and Dose Conversion Factors for Inhalation, Submersion, and Ingestion: Federal Guidance Report No. 11." (Washington, DC), no. EPA-5201188420, https://doi.org/10.2172/6294233.

Elzohery, R., D. Hartanto, F. Bostelmann, and W. A. Wieselquist. 2024. *SCALE Analyses of Scenarios in the High-Temperature Gas-Cooled Reactor Fuel Cycle.* Technical report ORNL/TM-2024/3536. Oak Ridge, TN: Oak Ridge National Laboratory.

Evans, T. M., A. S. Stafford, R. N. Slaybaugh, and K. T. Clarno. 2010. "Denovo: A New Three-Dimensional Parallel Discrete Ordinates Code in SCALE." *Nuclear Technology* 171 (2): 171–200. https://doi.org/10.13182/NT171-171.

Fuerst, T. F., C. N. Taylor, and P. W. Humrickhouse. 2021. *Tritium Transport Phenomena in Molten-Salt Reactors: Molten Salt Tritium Transport Experiment Design.* Technical report INL EXT-21-63108. Idaho Falls, ID: Idaho National Laboratory. https://www.osti.gov/biblio/1828384.

Gabraskas, D., T. Fei, and J. Jerden. 2020. *Technical Letter Report on The Assessment of Tritium Detection and Control in Molten Salt Reactors: Final Report.* Technical report ANL/NSE-20-15. Argonne, IL: Argonne National Laboratory. https://www.nrc.gov/docs/ML2015/ML20157A155.pdf.

Gehin, Jess C., and Jeffrey J. Powers. 2016. "Liquid Fuel Molten Salt Reactors for Thorium Utilization." *Nuclear Technology* 194 (2): 152–161. https://doi.org/10.13182/NT15-124.

Goluoglu, S., L. M. Petrie Jr, M. E. Dunn, D. F. Hollenbach, and B. T. Rearden. 2011. "Monte Carlo criticality methods and analysis capabilities in SCALE." *Nuclear Technology* 174 (2): 214–235. https://doi.org/10.13182/NT10-124.

Hartanto, D., F. Bostelmann, B. R. Betzler, K. B. Bekar, S. W. Hart, and W. A. Wieselquist. 2024. "SCALE Depletion Capabilities for Molten Salt Reactors and other Liquid-Fueled Systems." *Annals of Nuclear Energy* 196:110236. https://doi.org/10.1016/j.anucene.2023.110236.

Hartanto, D., G. Radulescu, F. Bostelmann, and W. A. Wieselquist. 2024. *SCALE Demonstration for Sodium-Cooled Fast Reactor Fuel Cycle Analysis.* Technical report ORNL/TM-2023/3214. Oak Ridge, TN: Oak Ridge National Laboratory. https://doi.org/10.2172/2341402.

Humphries, L. L., B. A. Beeny, F. Gelbard, D. L. Louie, J. Phillips, R. C. Schmidt, and N. E. Bixler. 2021. *MELCOR Computer Code Manuals - Vol. 1: Primer and Users' Guide Version 2.2.18019.* Technical report SAND2021-0726 O. Albuquerque, NM: Sandia National Laboratories. https://www.nrc.gov/docs/ML2104/ML21042B319.pdf.

Lo, A., F. Bostelmann, D. Hartanto, B. Betzler, and W. A. Wieselquist. 2022. *Application of SCALE to Molten Salt Fueled Reactor Physics in Support of Severe Accident Analyses.* Technical report ORNL/TM-2022/1844. Oak Ridge, TN: Oak Ridge National Laboratory. https://doi.org/10.2172/1897864.

ORNL. 2024. *Molten Salt Thermal Properties Database (MSTDB).* https://mstdb.ornl.gov/. Accessed: February 2024.

Pandya, T. M., S. R. Johnson, T. M. Evans, G. G. Davidson, S. P. Hamilton, and A. T. Godfrey. 2016. "Implementation, Capabilities, and Benchmarking of Shift, a Massively Parallel Monte Carlo Radiation Transport Code." *Journal of Computational Physics* 308:239–272. https://doi.org/10.1016/j.jcp.2015.12.037.

Peplow, D. E. 2011. "Monte Carlo Shielding Analysis Capabilities with MAVRIC." *Nuclear Technology* 174 (2): 289–313. https://doi.org/10.13182/NT174-289.

Pinto, J. Schorne. 2024. Private communication.

Robertson, R. C. 1965. *MSRE Design & Operations Report Part 1 Description of Reactor Design.* Technical report ORNL-TM-728. Oak Ridge, TN: Oak Ridge National Laboratory. https://doi.org/10.2172/4654707.

Robertson, R. C. 1971. *Conceptual Design Study of a Single-Fluid Molten-Salt Breeder Reactor.* Technical report ORNL-4541. Oak Ridge, TN: Oak Ridge National Laboratory. https://doi.org/10.2172/4030941.

Santora, J. 2022. "Assessment of Core Minimization Options for Breed-and-Burn Molten Chloride Fast Reactors." Master's thesis, Paul Scherrer Institute. https://doi.org/10.13140/RG.2.2.25119.84646.

Shaffer, J. H. 1971. *Preparation and Handling of Salt Mixtures for the Molten Salt Reactor Experiment.* Technical report ORNL-4616. Oak Ridge, TN: Oak Ridge National Laboratory. https://doi.org/10.2172/4074869.

Shaw, A., F. Bostelmann, D. Hartanto, E. Walker, and W. A. Wieselquist. 2023. *SCALE Modeling of the Sodium-Cooled Fast-Spectrum Advanced Burner Test Reactor.* Technical report ORNL/TM-2022/2758. Oak Ridge, TN: Oak Ridge National Laboratory. https://doi.org/10.2172/1991734.

Skutnik, S. E., and W. A. Wieselquist. 2021. *Assessment of ORIGEN Reactor Library Development for Pebble-Bed Reactors Based on the PBMR-400 Benchmark.* Technical report ORNL/TM-2020/1886. Oak Ridge, TN: Oak Ridge National Laboratory. https://doi.org/10.2172/1807271.

Thomas, S., and J. Jerden. 2020. *Mechanistic source term development for liquid fueled MSRs - Model Development Update.* Technical report ANL/CFCT-20/16. Argonne, IL: Argonne National Laboratory. https://doi.org/10.2172/1769029.

US NRC. 2020. *NRC Non-Light Water Reactor (Non-LWR) Vision and Strategy, Volume 3: Computer Code Development Plans for Severe Accident Progression, Source Term, and Consequence Analysis.* Technical report ML20030A178, Rev. 1. Rockville, MD: US Nuclear Regulatory Commission. https://www.nrc.gov/docs/ML2003/ML20030A178.pdf.

US NRC. 2021. *NRC Non-Light Water Reactor (Non-LWR) Vision and Strategy, Volume 5: Radionuclide Characterization, Criticality, Shielding, and Transport in the Nuclear Fuel Cycle.* Technical report ML21088A047, Rev. 1. Rockville, MD: US Nuclear Regulatory Commission. https://www.nrc.gov/docs/ML2108/ML21088A047.pdf.

Wagner, K., B. Beeny, T. Haskin, D. Luxat, and R. Schmidt. 2023. *MELCOR Accident Progression and Source Term Demonstration Calculations for a Molten Salt Reactor.* Technical report SAND2023-01803. Albuquerque, NM: Sandia National Laboratories. https://www.nrc.gov/docs/ML2311/ML23117A094.pdf.

Wagner, K., B. Beeny, and D. Luxat. 2022. *MELCOR Accident Progression and Source Term Demonstration Calculations for a HTGR.* Technical report SAND2022-2750. Albuquerque, NM: Sandia National Laboratories. https://www.osti.gov/biblio/1854083.

Wagner, K., B. Beeny, and D. Luxat. 2023. *MELCOR Accident Progression and Source Term Demonstration Calculations for a Sodium Fast Reactor (SFR).* Technical report SAND2023-10830. Albuquerque, NM: Sandia National Laboratories. https://www.nrc.gov/docs/ML2328/ML23285A093.pdf.

Wagner, K., C. Faucett, R. Schmidt, and D. Luxat. 2022. *MELCOR Accident Progression and Source Term Demonstration Calculations for a Heat Pipe Reactor.* Technical report SAND2022-2745. Albuquerque, NM: Sandia National Laboratories. https://www.osti.gov/biblio/1854082.

Wagner, K., T. Haskin, B. Beeny, F. Gelbard, and D. Luxat. 2022. *MELCOR Accident Progression and Source Term Demonstration Calculations for a FHR.* Technical report SAND2022-2751. Albuquerque, NM: Sandia National Laboratories. https://www.osti.gov/biblio/1854081.

Walker, E., S. E. Skutnik, W. A. Wieselquist, A. Shaw, and F. Bostelmann. 2021. *SCALE Modeling of the Fast-Spectrum Heat Pipe Reactor.* Technical report ORNL/TM-2021/2021. Oak Ridge, TN: Oak Ridge National Laboratory. https://doi.org/10.2172/1871124.

Wieselquist, W., and R. A. Lefebvre. 2023. *SCALE 6.3.1 User Manual.* Technical report ORNL/TM-SCALE-6.3.1. Oak Ridge, TN: Oak Ridge National Laboratory. https://doi.org/10.2172/1959594.

Williams, D. F., L. M. Toth, and K. T. Clarno. 2006. *Assessment of Candidate Molten Salt Coolants for the Advanced High-Temperature Reactor (AHTR).* Technical report ORNL/TM-2006/12. Oak Ridge, TN: Oak Ridge National Laboratory. https://doi.org/10.2172/885975.